Material properties and applications of mechanically interlocked polymers

Laura F. Hart[1,4], *Jerald E. Hertzog*[2,4], *Phillip M. Rauscher*[1,4], *Benjamin W. Rawe*[1,4], *Marissa M. Tranquilli*[2,4] *and Stuart J. Rowan*[1,2,3]✉

Abstract | Mechanically interlocked polymers (MIPs), such as polyrotaxanes and polycatenanes, are polymer architectures that incorporate a mechanical bond. In a polyrotaxane, the mechanical bond is the result of a linear dumbbell component threaded through a ring, while in a polycatenane, it is the consequence of interlocked ring components. The interlocked nature of these architectures can result in high degrees of conformational freedom and mobility of their components, which can give rise to unique property profiles. In recent years, the synthesis and studies of a range of MIPs has allowed researchers to build an initial understanding of how incorporating mechanical bonds within a polymer structure impacts its material properties. This Review focuses on the understanding of these structure–property relationships, with an outlook towards their applications, specifically, focusing on four main classes of MIPs: polyrotaxanes, slide-ring gels, daisy-chain polymers and polycatenanes.

A key feature that controls the properties of a polymeric material is its architecture. Beyond the conventional linear polymer, architectures such as branched, cyclic, bottlebrush, star and block copolymers have expanded the property profile of polymeric materials and offered opportunities for polymer research and applications. Recently, the polymer field has seen the emergence of a new class of polymer architecture: mechanically interlocked polymers (MIPs), which are polymers that include a mechanical bond.

The mechanical bond itself is not a new idea, occurring when two (or more) molecular components are constrained in space without being covalently bonded together (FIG. 1). Mechanically interlocked molecules (MIMs) possess large conformational freedom while maintaining a permanent spatial association between the components[1–4]. MIMs have played an important role in the field of molecular switches and molecular machines, and were recognized in 2016 with the Nobel Prize in Chemistry being awarded to Jean-Pierre Sauvage, Sir J. Fraser Stoddart and Bernard L. Feringa[5–8]. However, MIMs are not confined to this field, and have been explored in applications that range from drug delivery to catalysis[9–15].

MIPs present an attractive frontier in polymer science, as the presence of the mechanical bond allows for unprecedented degrees of motion within the polymer architecture. Conceptually, there are a myriad of ways the mechanical bond can be incorporated into polymer architectures (FIG. 1), and these unique and varied structures can enable property profiles that have never been seen before.

The most common MIP is based on the rotaxane architecture: a ring (macrocycle) threaded onto a dumbbell-like component (FIG. 1a), where the ring is able to slide back and forth along the dumbbell component but is prevented from dethreading by the presence of bulky stoppers. A polymeric analogy to this would be the main-chain polyrotaxane (FIG. 1b), in which the ring(s) are trapped on the polymer backbone and can undergo a similar sliding motion over a much longer distance. Thus, by expanding or limiting the range of the rings' sliding motion (for example, by controlling the length of the polymer backbone or the number of rings on it), the properties of the polyrotaxane can be tuned. Another important class of MIPs is slide-ring materials (SRMs), which are polymer networks where the crosslink itself is a rotaxane moiety. The term slide-ring gels, SRGs, is also commonly used to describe these materials, particularly if the network is swollen with a solvent. The most common of these systems contain figure-of-eight crosslinks (FIG. 1c) and the resulting MIP networks have mobile junctions that can slide freely along the polymer backbone. The final class of polyrotaxanes to be discussed are 'daisy-chain' architectures, which feature interlocked monomeric units composed of two of the key polyrotaxane elements (the ring and the thread) covalently bound together; the simplest form of this structure is the dimeric cyclic [*c*2]daisy chain (FIG. 1d).

The other main class of MIPs is mechanically interlocked rings, or catenanes (such as a [2]catenane, FIG. 1e). This chain-link structure can be incorporated into a polymer in many ways: as monomeric subunits

[1]*Pritzker School of Molecular Engineering, University of Chicago, Chicago, IL, USA.*

[2]*Department of Chemistry, University of Chicago, Chicago, IL, USA.*

[3]*Chemical and Engineering Sciences, Argonne National Laboratory, Lemont, IL, USA.*

[4]*These authors contributed equally: Laura F. Hart, Jerald E. Hertzog, Phillip M. Rauscher, Benjamin W. Rawe, Marissa M. Tranquilli.*

✉*e-mail: stuartrowan@uchicago.edu*

https://doi.org/10.1038/s41578-021-00278-z

(poly[2]catenane), pendant moieties or even composing the entirety of the polymer (polymeric [2]catenane, Olympic gel, poly[*n*]catenane (FIG. 1e)). Mechanically bonded rings do not allow for the long-range translational motion present in the polyrotaxanes; however, the components of a catenane possess several unusual degrees of freedom, such as elongation, twisting and rotating motions (FIG. 1e).

Although MIP synthesis remains a challenge, developments have been made over the years that have allowed access to a range of MIPs[16,17]. In this Review, we will focus on polyrotaxanes, SRMs and polycatenanes to examine the current understanding of how the mechanical bond impacts the properties of a polymeric material and the potential applications of such materials. Although syntheses will be touched upon, it will not be the focus of this Review and readers interested in synthetic approaches to MIPs are directed elsewhere[18–21]. Other classes of interlocked polymers, such as pseudopolyrotaxanes or knot-based materials[10,20], will not be discussed herein.

Polyrotaxane materials

Rotaxane moieties can be incorporated into macromolecules in a variety of ways (FIG. 2a). The resulting architectures include main-chain polyrotaxanes (in which the polymer backbone is part of the rotaxane moiety, either as the thread or the ring component (FIG. 2a, left)), side-chain polyrotaxanes (FIG. 2a, centre) and polyrotaxanes in which the mechanical bond is incorporated into the polymer backbone, such as the poly[2]rotaxanes (top right) and poly[3]rotaxanes (FIG. 2a, bottom right). Although these architectures have been synthesized[20,22], it is the main-chain polyrotaxanes that have provided

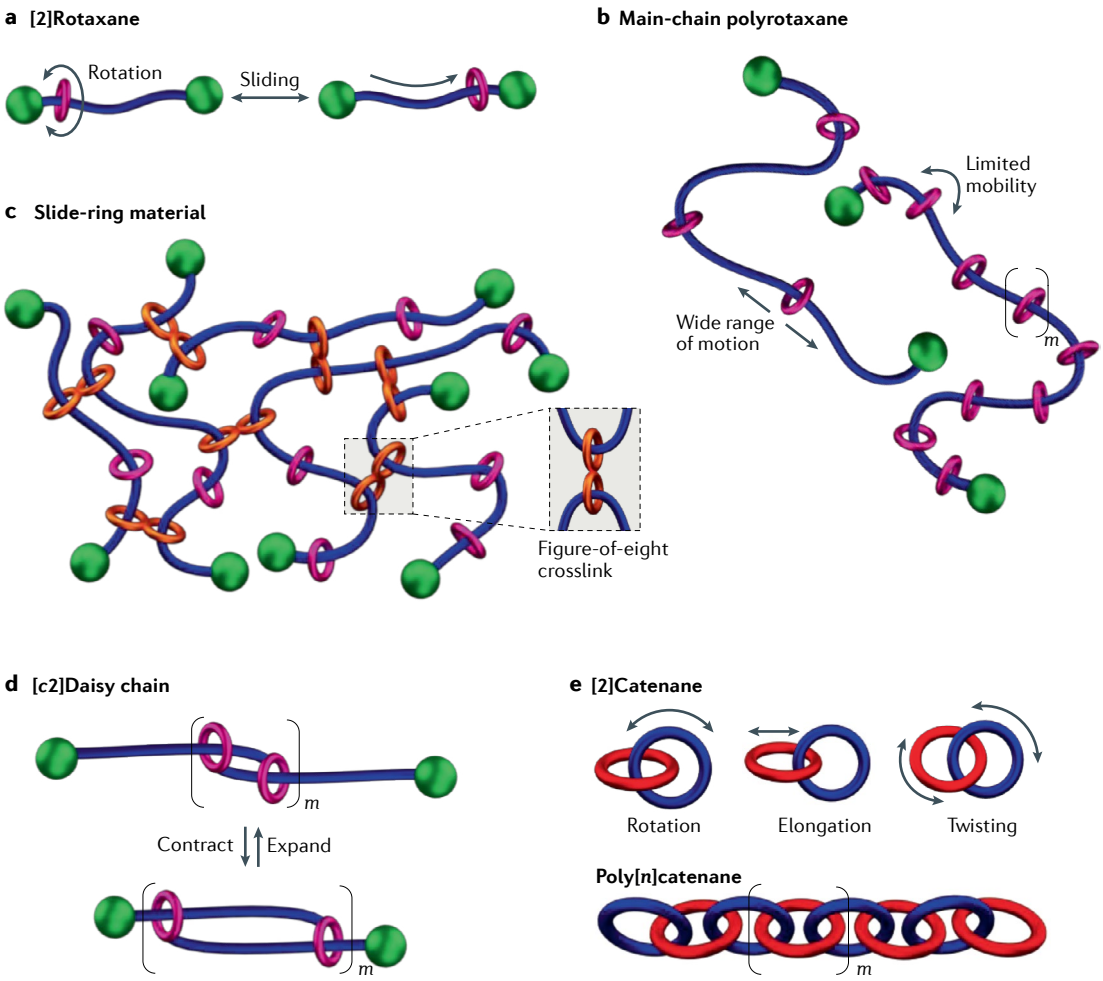

Fig. 1 | **Mechanically interlocked molecules and polymers. a** | A schematic of a [2]rotaxane, demonstrating the translational motion of a free ring along the dumbbell component. **b** | In a main-chain polyrotaxane, the *m* rings can exhibit translational motions similar to their small molecule counterparts but potentially over longer distances, depending on, for example, the number of rings. **c** | Interchain crosslinking of a main-chain polyrotaxane through the rings yields a slide-ring material with mobile figure-of-eight crosslinks (orange). **d** | The expansion and contraction motions of a polymeric [c2]daisy chain. **e** | A [2]catenane is capable of rotation, elongation and twisting motions that can be expanded to *n* times in a poly[*n*]catenane, a polymer consisting only of *n* interlocked rings.

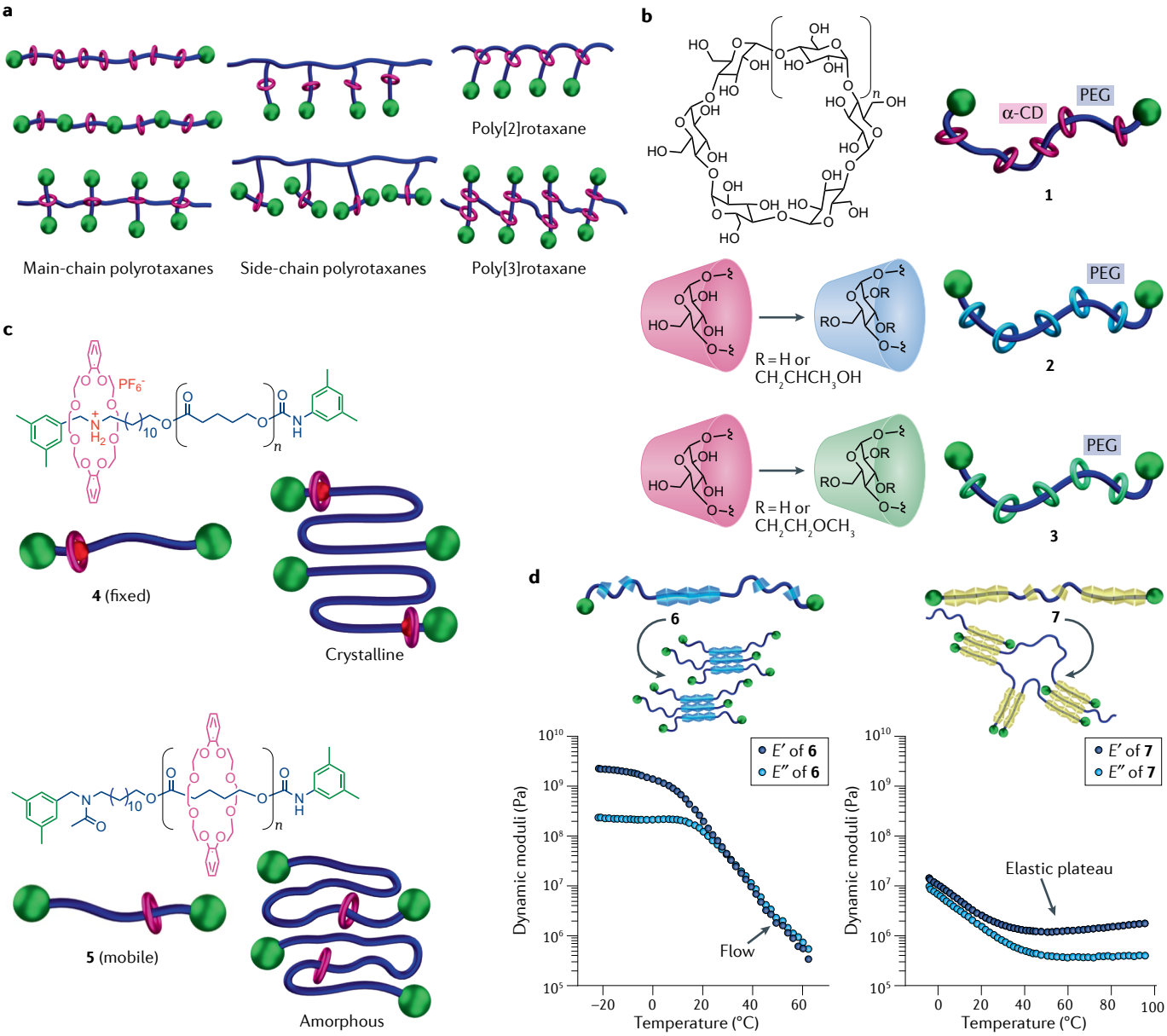

Fig. 2 | **Polyrotaxanes. a** | A selection of polyrotaxane architectures that includes main-chain polyrotaxanes (left), side-chain polyrotaxanes (centre), poly[2]rotaxanes (or daisy chains) (top right) and poly[3]rotaxanes (bottom right). **b** | Polyrotaxanes are often synthesized using cyclodextrin (top left), which is commercially available in three ring sizes, α, β and γ, where $n = 1$, 2 or 3 anhydroglucopyranoside units. A main-chain polyrotaxane composed of poly(ethylene glycol) (PEG) threaded through α-cyclodextrin (α-CD) (**1**) (top, right). Partial hydroxypropylation of α-CD is used to access the PEG-based polyrotaxane, **2** (middle row). Partial methoxyethylation of α-CD is used to access the PEG-based polyrotaxane, **3** (bottom row). **c** | Chemical structure of the ammonium-containing polycaprolactone-based polyrotaxane **4** with dibenzo[24]crown-8 and the related amine-protected polyrotaxane **5** with schematics highlighting their crystallization behaviour. **d** | Cartoons showing the CD distribution in **6**, its proposed self-assembly and the temperature-sweep dynamic mechanical analysis data of a **6** film (left), and cartoons showing the CD distribution in **7**, its proposed self-assembly and the temperature-sweep dynamic mechanical analysis data of a **7** film (right). Panel **d** reprinted with permission from REF.[45], ACS.

the most insight into how an interlocked architecture impacts material properties.

Main-chain polyrotaxanes

As in traditional polymers, the chemistry and structure of the backbone plays a role in the behaviour of polyrotaxanes. However, their properties are also impacted by the ring(s) and stopper(s), as well as the interactions between these interlocked components. These relationships have been most extensively characterized in main-chain polyrotaxanes (FIG. 2a, left).

The first report of a main-chain polyrotaxane was by Harrison and Harrison in 1967 (REF.[23]). However, the field did not gain traction until 1992, when Wenz and Keller reported the threading of poly(iminooligomethylene)s through α-cyclodextrin (α-CD) rings[24] and Harada reported the threading of poly(ethylene glycol) (PEG) through α-CDs[25]. The PEG and α-CD pseudopolyrotaxane assembly is highly efficient and driven by a combination of hydrophobic interactions (between the polymer chain and the hydrophobic pocket of the CD) and hydrogen bonding between

adjacent CDs[26]. The polyrotaxane **1** is formed when a stoppering reaction is used to 'trap' the α-CD rings on the polymer backbone[27] (FIG. 2b, top). In addition to ease of synthesis, CDs are commonly used in polyrotaxanes because they are commercially available in three sizes that vary in the number of α-D-glucopyranoside units (FIG. 2b, α-CD ($n = 1$), β-CD ($n = 2$) and γ-CD ($n = 3$)). As such, CD-based polyrotaxanes are the most studied, producing valuable insights into polyrotaxane structure–property relationships.

In **1**, the α-CD rings play a significant role in the properties of the material: hydrogen bonding between the rings favours their aggregation on the polymer backbone, resulting in semi-crystalline materials, limiting ring mobility along the polymer backbone[28]. However, these hydrogen bonds can be disrupted, either by introducing a hydrogen-bond-competing solvent or through partial hydroxypropylation or methoxyethylation of the CD rings, resulting in more soluble amorphous polyrotaxanes (**2** and **3**) (FIG. 2b) with enhanced ring translational mobility[28,29] (FIG. 1b). Studies have focused on how this mobility and the resulting material properties are affected by parameters such as ring–backbone interactions, ring–ring interactions, polymer concentration and ring coverage (calculated as either the number of rings per repeat unit or the percent coverage of the backbone by the rings)[30–34].

The mobility and placement of the rings are controlled, in part, by the inherent interactions between the ring and polymer backbone. For instance, the energy barrier resulting from attractive interactions between the CD and PEG backbone in **1** leads to slower diffusion of the α-CD along the PEG backbone compared with unthreaded (free) CD[32]. Furthermore, the presence of the rings impacts the polymer backbone by, for example, decreasing the flexibility of the polymer with increasing ring coverage, leading to stiffer polyrotaxanes[26,35]. The effect of ring–backbone interactions has been studied in polyrotaxanes with rings other than CD, for instance, crown ethers. Early examples of polyrotaxanes based on crown ethers include those reported by Gibson, in which the stopper groups are incorporated into the polymer backbone[36–43]. These polyrotaxanes were synthesized by copolymerizing an alkyl diol monomer and a bulky diol monomer with either diacid chloride monomers (forming polyesters) or diisocyanate monomers (forming polyurethanes) in the presence of a high concentration of [30]crown-10 rings. The sliding mobilities of the crown ethers in the resulting polyrotaxanes vary based on the differing backbone chemistries. In the polyester-based polyrotaxane, the crown ether rings move freely between the stoppers and appear as a range of broad signals in the ^{1}H NMR spectrum. In contrast, the polyurethane-based polyrotaxanes exhibit hydrogen bonding between the ring and the polymer backbone NH groups (in $CDCl_3$), which restricts ring mobility, as demonstrated by the methylene groups of the crown ethers appearing as a single peak in the NMR spectrum. In a hydrogen-bond-competing solvent (for example, d^6-dimethyl sulfoxide (DMSO)), the hydrogen bonding is 'switched off', increasing ring mobility and resulting in the methylenes showing up as a broad range of peaks in the ^{1}H NMR spectrum, similar to systems with no hydrogen bonding present.

This difference in ring mobility is also seen in the solid-state properties of similar crown-ether-based polyester and polyurethane polyrotaxanes[36,40,42,43]. The polyester polyrotaxanes exhibit two melting-to-crystallization transitions (as determined by differential scanning calorimetry), suggesting that the rings are mobile enough to phase separate and allow the rings and polymer chains to crystallize separately. In contrast, hydrogen bonding in the polyurethanes results in a single-phase material that only exhibits one glass transition temperature (T_g).

The effect of ring mobility on the solid-state properties of a polyrotaxane can even be observed with just a single mobile ring present. For example, Takata and colleagues[44] synthesized macromolecular [2]rotaxanes using poly(δ-valerolactone) with a single secondary ammonium binding site on the thread component (M_n ca. 2,300 g mol^{-1}) and [24]crown-8 as the ring (**4**, FIG. 2c, top). The secondary ammonium site interacts favourably with the crown ether ring, limiting its motion and allowing crystallization of the poly(δ-valerolactone) segment in **4**. However, if the secondary amine is acetylated (**5**), the hydrogen bonding between the ring and the thread is 'switched off', increasing ring mobility and disrupting crystallization, resulting in an amorphous material[44] (FIG. 2c, bottom).

In addition to ring mobility, how the rings are distributed along the polymer backbone can affect the solid-state properties. For example, Ito and colleagues[45] studied a poly(ethylene oxide)-*b*-poly(propylene oxide)-*b*-poly(ethylene oxide) (PEO–PPO–PEO) triblock main-chain polyrotaxane with either fully functionalized hydroxypropyl-β-CDs (100% HP-β-CDs, **6**) or trimethylsilyl-functionalized hydroxypropyl-β-CDs (100% TMS-β-CDs, **7**) as the ring components. In **6**, the β-CDs preferentially reside on the inner PPO block on account of more favourable hydrophobic interactions with PPO than PEO[46] (FIG. 2d, left). In contrast, the TMS-β-CDs in **7** reside on the PEO end blocks in order to shield the polar PEO segments from the hydrophobic TMS-β-CD outer wall[44] (FIG. 2d, right). In both polymers, the CDs form crystalline domains; however, the different positioning of the CDs along the polymer backbone results in drastically different mechanical properties. In **6**, the concentration of the CDs on the central PPO block results in discrete crystalline assemblies and, as a result, the films exhibit fluid-like behaviour above T_g, as shown by dynamic mechanical analysis (FIG. 2d, left). In **7**, the CDs are concentrated on the outer PEO blocks so that the crystalline CD domains are bridged by polymer chains, resulting in an elastic plateau even above T_g (FIG. 2d, right).

CD crystallization in polyrotaxanes has also been used by Ke and colleagues to obtain 3D-printed cubic wood-pile lattices[47–49]. In these materials, obtained from the chemical photocrosslinking of main-chain pseudopolyrotaxanes, the α-CDs hydrogen bond into tubular arrays, which form hexagonal crystalline domains that function as physical crosslinking sites[47,48]. Varying pH (FIG. 3a, top) or solvent type (FIG. 3a, bottom) can

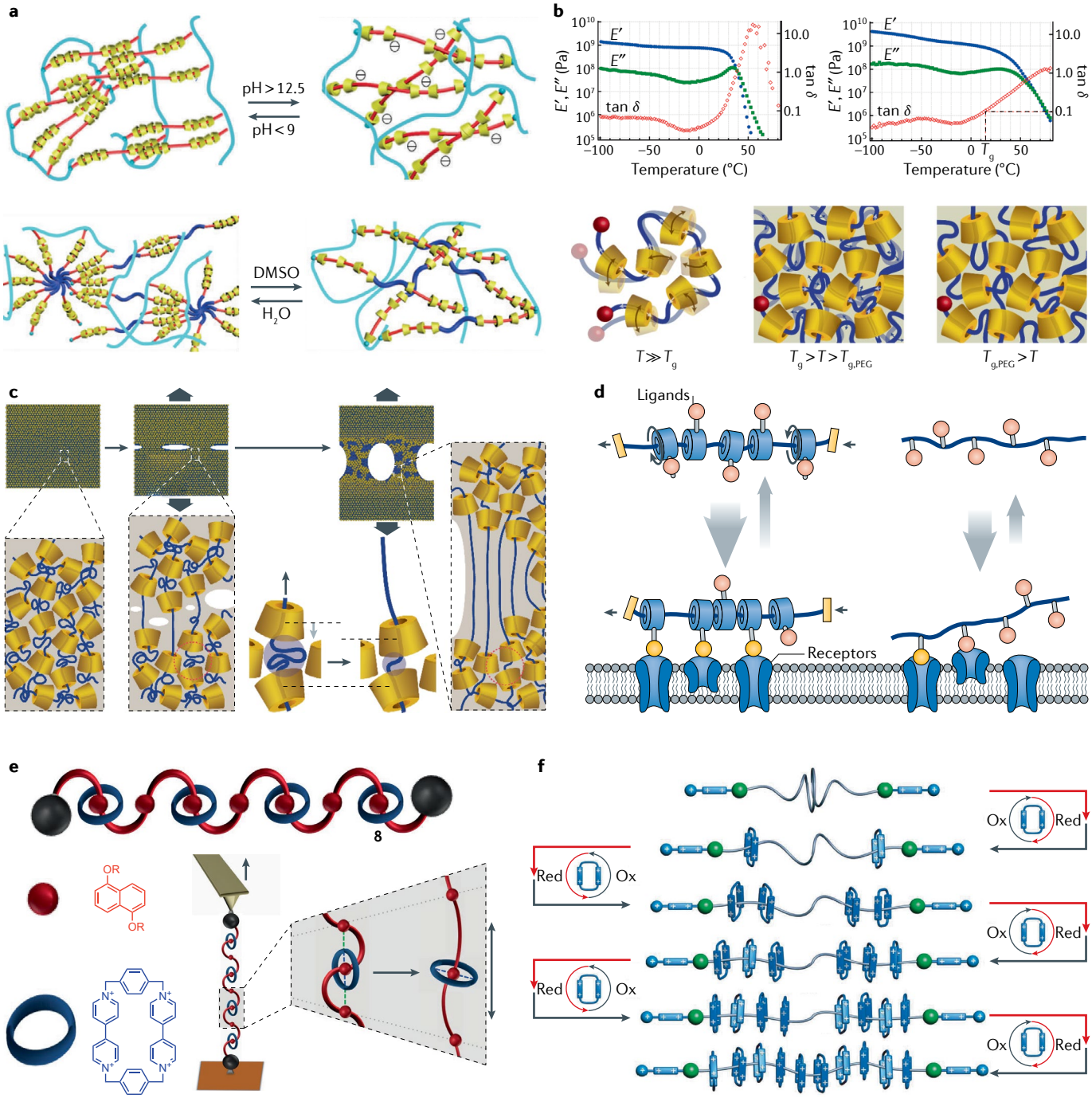

Fig. 3 | **Main-chain polyrotaxane properties and behaviour. a** | Cartoon showing the effect of pH (top) or solvent change (bottom) on the aggregation of threaded cyclodextrins (CDs) in a photocrosslinked polyrotaxane. **b** | Temperature dependence of tensile storage modulus (*E′*), loss modulus (*E″*) and loss tangent (tan *δ*) of α-CD (46% methoxylated) glass (top left) and **3** polyrotaxane glass (poly(ethylene oxide) backbone, 25% ring coverage, 46% methoxylated α-CD rings)) (top right). Cartoon showing the vitrification of CD rings in **3**, highlighting the poly(ethylene glycol) (PEG) chain mobility above $T_{g,PEG}$ (bottom). **c** | Scheme showing how the structure of a polyrotaxane glass (**2** and **3**) changes during stress below the glass transition temperature T_g: homogenous CD distribution before stress (left), fragmentation of CD framework (centre), stress-induced translational motion of the threaded PEG chains (bottom right) and microscopic phase separation of backbone PEG chains and CD framework (right). **d** | Cartoon highlighting the difference in multivalent binding of the more mobile ligands on polyrotaxane rings (left) versus them directly conjugated to a polymer backbone (right). Yellow ligands indicate successful ligand–receptor binding. **e** | Cartoon image of folded structure of **8** with blue cyclobis(paraquat-p-phenylene) (CBPQT) rings and red 1,5-dioxynaphthalene backbone polymer (top). Cartoon showing breaking of π-stacking between the CBPQT rings and naphthalene backbone in the foldamer during a single-molecule atomic force microscopy experiment (bottom). **f** | Cartoon showing the stepwise addition of CBPQT rings (up to 10) onto a PEG backbone using chain-end redox-active molecular pumps. DMSO, d^6-dimethyl sulfoxide. Panel **a** adapted with permission from REF.[47], RSC, and REF.[48], Wiley-VCH. Panel **b** reprinted with permission from REF.[29], ACS. Panel **c** reprinted with permission from REF.[50], ACS. Panel **d** reprinted with permission from REF.[77], Wiley-VCH. Panel **e** reprinted from REF.[91], Springer Nature Limited. Panel **f** reprinted with permission from REF.[95], AAAS.

disrupt (or reform) these physical crosslinks, leading to a decrease (or increase) in moduli, allowing access to shape-memory properties. Such shape-memory behaviour combined with the lattice structure allows the material to actuate in a controlled manner, exemplified by the lifting of a coin upon reformation of the crystalline CD domains. Related work using the lower critical solution temperature behaviour of methylated CDs showed similar actuation behaviour upon temperature cycling[49].

All the films discussed so far were investigated above T_g (which allows movement of both polymer chains and rings), but polyrotaxanes may also have interesting properties in the glassy regime below T_g. Unfortunately, the rings in CD-based polyrotaxanes crystallize rather than vitrify; however, crystallization can be inhibited by partial functionalization of the CD rings, allowing access to polyrotaxane glasses. For example, glassy polyrotaxane **3** consists of a PEO backbone ($M_n = 20{,}000\ g\ mol^{-1}$) threaded through partially 2-methoxyethylated α-CD (46% hydroxy groups reacted and a CD to repeat unit ratio of 1:8 (25% coverage)). As the CDs comprise ca. 80 wt% of the material, there is a T_g at ca. 8 °C, comparable to the neat 2-methoxyethylated α-CDs (FIG. 3b, top left). However, **3** also exhibits a secondary relaxation (sub-relaxation) at ca. −30 °C (FIG. 3b, top right), close to the T_g of PEO (ca. −35 °C). Raising the temperature above this secondary relaxation reduces the modulus to about a third of its value at −100 °C (REF.[29]). This sub-relaxation is linked to the interlocked architecture and is consistent with the PEG backbone sliding through the glassy CD framework (FIG. 3b, bottom). As a result, these polyrotaxane glasses can be extremely ductile because the polymer chains slide through the rings at points of high stress, allowing material deformation and resulting in enhanced toughness[50] (FIG. 3c). Further research showed similar effects in **2** and demonstrated that the properties of both **2** and **3** could be tuned by changing either the amount of chemically modified hydroxy groups on the CD or the ring coverage. For instance, less 'fragile' glass-formers with reduced T_g and less cooperative dynamics were obtained by increasing the chemical modification of the CDs, which mitigates ring–ring interactions[51], while increased CD coverage results in an additional relaxation slightly above T_g, attributed to correlated motions of neighbouring CDs on the polyrotaxane backbone[52].

The encapsulation of a polymer by rings results in reduced interpolymer chain interactions. This effect has been used to synthesize polyrotaxanes that can act as molecular wires[53]. Conjugated polymers have long been candidates for the development of molecular-scale wires; unfortunately, strong interchain interactions make it difficult to isolate single polymers and the conformational entropy of the polymer disfavours extended, straight chain configurations, limiting conjugation within the backbone[54]. Sheathing of a conjugated polymer with rings drastically improves its overall rigidity and 'insulates' the threaded polymer chain. A number of conducting polymers have been investigated in such polyrotaxanes[55], including poly(phenylenevinylene)[56], polyfluorene[57], poly(paraphenylene)[58], poly(diphenylenevinylene)[59] and polythiophene[60]. While the most common ring component in these polyrotaxanes is CD, other rings such as cyclophanes[61] and cucurbiturils[62] have been reported. Most studies on conjugated polyrotaxanes are focused on their optical properties. For example, CD-based conjugated polyrotaxanes exhibit sharper ultraviolet (UV)–visible spectra, blue-shifted emission spectra, as well as higher quantum yields relative to their unthreaded conjugated polymer counterparts[54,55]. In these systems, the rings separate the polymer chains, preventing aggregation (and quenching) and leading to longer lifetime excited states. In addition, threaded rings cause increases in the persistence length of the backbone, stretching the polymer out and resulting in more extended, near-planar conformations, important for enhancing the conjugation along the backbone[54,63,64]. For example, poly(4,4′-diphenylenevinylene) polyrotaxanes with varying β-CD ring coverage (between 0% and 82%) showed an increase in the electroluminescence quantum efficiency and solid-state photoluminescence with increasing coverage[65]. Ring size is also an important feature in these polyrotaxanes; systems with larger rings (for example, γ-CD versus α-CD) exhibit greater fluorescence quenching by methylviologen in aqueous solution[66]. It was suggested that these larger rings have greater mobility along the polyrotaxane backbone, allowing larger aggregate formation. Preliminary investigations into the electrical behaviour of these polyrotaxanes have shown that their conductivity can be orders of magnitude higher than the unthreaded conjugated backbone[67], although investigations in this area are primarily focused on pseudopolyrotaxanes[68,69]. Nonetheless, such pseudopolyrotaxane studies have shown that the hole mobility along a threaded poly(phenylene ethynylene) backbone can be similar to amorphous silicon, highlighting the potential of these MIPs as well-insulated organic semiconductors[70,71].

Main-chain CD polyrotaxanes have also been investigated as functional biomaterials[72–77], aided by the fact that the components of **1** (α-CD and PEG) are approved by the US Food and Drug Administration for drug use[78]. For example, controlled release of drugs covalently attached to the CD rings can occur with selective removal of the stopper groups[72–75]. For gene delivery, CDs functionalized with cationic groups can form complexes with anionic nucleic acids, either DNA or RNA. Owing to the mobility of the positively charged CD rings, these polyrotaxane/nucleic acid complexes are much stronger than comparable systems comprising linear cationic polymers and nucleic acids[79,80]. Upon entering the cell, the stopper groups can be selectively removed, resulting in decomplexation and subsequent delivery of the nucleic acid payload[72–75].

Ring mobility in polyrotaxanes has also been used to enhance biological targeting of synthetic systems. In nature, multivalency is commonly used to enhance the molecular recognition of weak ligand–receptor interactions[81]. However, this typically requires the binding sites to be precisely arranged in space. When ligands are attached to the polyrotaxane rings, the ring mobility (both translational and rotational) allows the ligands to arrange themselves to optimize the multivalent interactions[76,77]. Such polyrotaxanes exhibit faster

and more efficient multivalent binding to receptor proteins when compared with ligands tethered to standard covalent polymers[82,83] (FIG. 3d).

Building on the previously mentioned ability of MIMs to act as switches and machines[84,85], main-chain polyrotaxane architectures have also attracted attention as polymer-based switches and machines[86,87]. For instance, Stoddart and colleagues developed polyrotaxane 'foldamers' capable of concerted motion at the macromolecular scale[87–90]. These polyrotaxanes (**8**) use π-stacking interactions between a cyclobis(paraquat-*p*-phenylene) ($CBPQT^{4+}$) rings and a 1,5-dioxynaphthalene backbone polymer (FIG. 3e) to fold in a specific manner, which results in a conformation that is ca. 15% shorter and 92% wider than the free backbone[87]. Single-molecule force spectroscopy was used to observe the transition between folded and unfolded states under applied force and showed that **8** could exert forces of up to 50 pN (under a load of 150 pN) during folding[91] (FIG. 3e). Furthermore, π-stacking rupture events during extension can be observed with dynamic force spectroscopy, confirming the folded structure[92]. These measurements also implied a rapid reformation of the folded structure because the interlocked structure prevents disassembly of the components.

Strides towards accessing polyrotaxanes machines have been made by Stoddart and colleagues through the synthesis of a high-energy polyrotaxane through successive controlled pumping of $CBPQT^{4+}$ rings onto a polymeric chain[93–95] (FIG. 3f). Each chain end contains a viologen unit sandwiched between a pyridinium group (that acts as a Coulombic barrier) and an isopropyl group (acting as a steric speed bump)[93–95]. Rings can be added to the polyrotaxane by reducing the viologen units and $CBPQT^{4+}$ ring, allowing threading of the ring onto the viologen, driven by the formation of a trisradical tricationic association complex. Reoxidation then forces the ring over the isopropyl speed bump on account of Coulombic repulsions, resulting in a stable polyrotaxane. This ring-addition ratchet mechanism can be repeated to drive the controlled pumping of between 2 and 10 rings onto the polymer backbone, resulting in highly charged, high-energy systems with the potential to perform work.

Slide-ring materials

Crosslinking a polymeric material gives rise to an enhanced property profile that includes higher modulus and elasticity, solvent resistance, lower rates of creep and improved temperature stability relative to its uncrosslinked counterpart[96]. Although crosslinking is commonly achieved through chemical bonds or physical interactions, it can also be realized with mechanical bonds. For instance, crosslinking polyrotaxanes by covalently linking their rings results in the formation of SRMs[97]. As the polymer chains are not fixed by permanent covalent bonds, the interlocked crosslinking site has the ability to slide along the polymer backbone, akin to a pulley (FIG. 4a), a process that can dramatically affect material properties. In chemical gels, fixed (covalent) crosslinks are not distributed evenly throughout the material and, upon deformation, the shorter strands can rupture, leading to mechanical failure (FIG. 4b, left). However, mobile interlocked crosslinks allow polymer chains to slide through the network like a pulley system, allowing dissipation of stresses in a cooperative manner (FIG. 4b, right). Such interlocked networks have been broadly classified as SRMs, and the mobility of their crosslinks imbues them with new property profiles.

Molecular processes in SRMs. The first and most studied class of SRMs incorporates interlocked crosslinks by covalently bonding rings from different polyrotaxanes, yielding 'figure-of-eight' topological crosslinks. The quintessential example of a SRM, **9**, can be prepared by crosslinking the α-CD rings on **1** (REF.[97]) (FIG. 4c). Importantly, this synthetic protocol results in both figure-of-eight crosslinks and residual uncrosslinked rings in the polymer network; the latter also plays a role in the properties of these SRMs. Such polymer networks exhibit an impressive property profile; for example, **9** can absorb 24,000 times its mass in water and extend to 24 times in length without hysteresis[13,97–99]. The interlocked crosslinking architecture also influences the mechanical properties[54], exemplified by the stress–strain behaviour (FIG. 4d). Although fixed-crosslinked networks reveal the typical 'S'-shaped curves, SRMs have a 'J'-shaped profile with lower elastic (Young's) modulus and much greater strain-at-break. Other properties such as fracture behaviour[100] and strain recovery[54] are also affected, as discussed later.

In the past two decades, there have been substantial investigations into the molecular processes and structure–property relationships of these topological materials[101–105]. The elasticity of conventional polymer networks arises from the conformational entropy of polymer segments between fixed crosslinks. Although this conformational entropy also plays a role in SRMs, two additional molecular mechanisms are at work: first, crosslink mobility and, second, configurational entropy of the uncrosslinked rings (if present). These mechanisms are unique to SRMs and, in combination with traditional network elasticity, lead to their exceptional properties. Although this section focuses on figure-of-eight SRMs that contain solvent (namely, SRGs), the concepts are applicable to SRMs with different crosslink architectures (to be discussed later) with or without solvent.

Let us first consider the impact of crosslink mobility on the behaviour of polymer networks. If crosslinks in polymer networks are fixed, they are constrained to a specific point on the polymer chains. However, in SRMs, these constraints are lifted because the crosslinks are free to slide along the backbone; from a thermodynamic perspective, the removal of any constraint always allows the system to relax to a state of lower free energy. In SRMs, this leads to a lower elastic (Young's) modulus. The concept of mobile crosslinks originated in the study of rubber elasticity and trapped entanglements, which are formed by the concatenation of network loops during the crosslinking process[106–113]. The point of contact between the two loops acts as a sort of crosslink whose position is not fixed, similar to the figure-of-eight crosslinks in SRMs. Thus, a number of slip-link models were developed to explain the non-linear elasticity of rubbers[106–113].

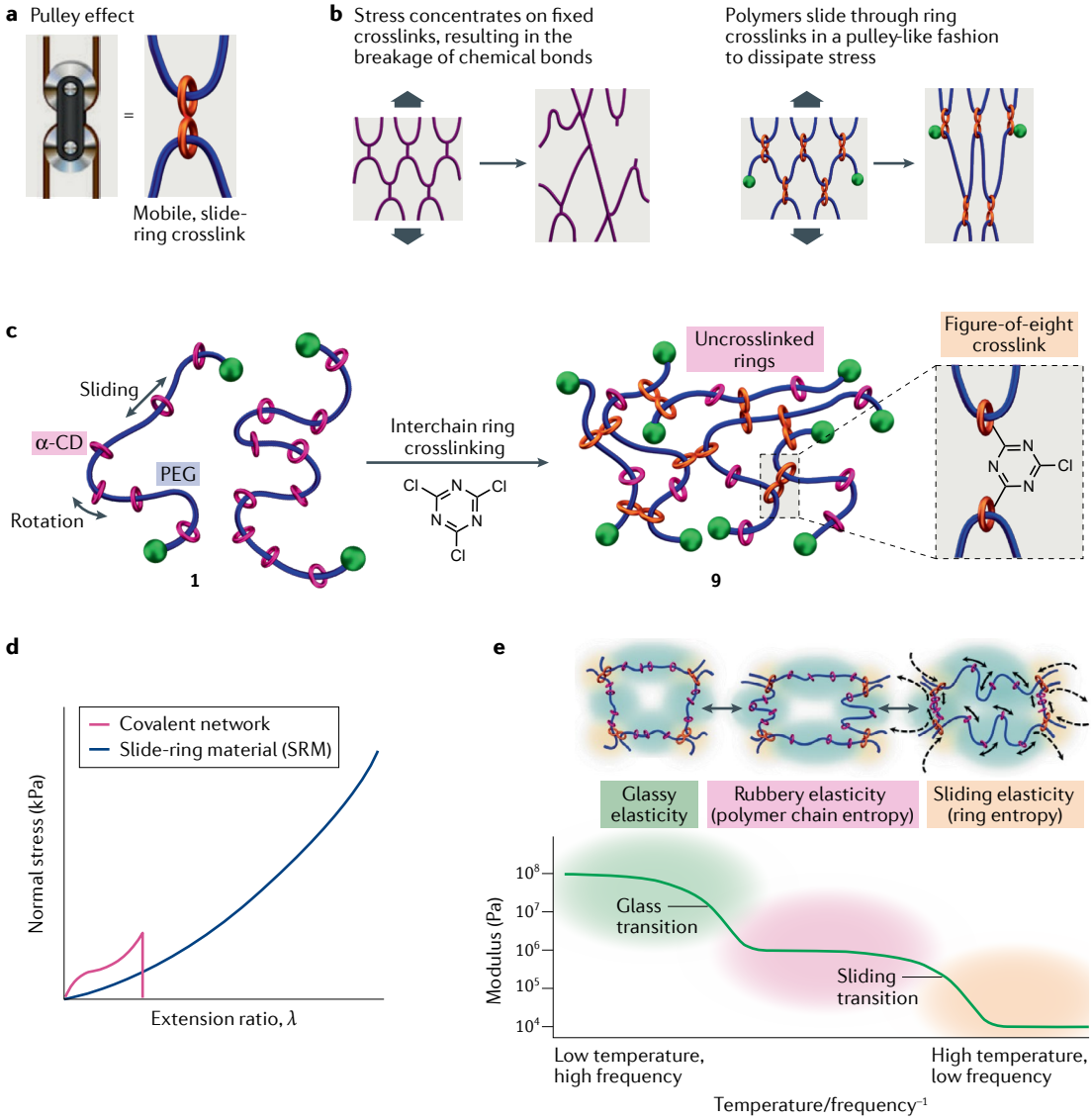

Fig. 4 | **'Pulley effect' in figure-of-eight slide-ring materials. a** | Visualization of the pulley effect that has been used to describe the mobile, slide-ring crosslinks (orange) of slide-ring materials (SRMs). **b** | The effects of strain on a fixed-crosslinked network (left), where short network strands tend to rupture under strain, and a SRM (right), where the pulley effect allows for dissipation of stress as polymer chains slide through the crosslinked rings in a cooperative manner, akin to a pulley system. **c** | Synthesis of a SRM (**9**) via interchain ring crosslinking of hydroxy groups on the α-cyclodextrins (α-CDs) (pink) in **1** with cyanuric chloride, resulting in figure-of-eight crosslinks (orange) and residual, uncrosslinked α-CDs (pink). **d** | Schematic comparing the idealized tensile properties of figure-of-eight SRMs and conventional polymer networks with fixed crosslinks. **e** | Oscillatory shear rheology of **9** shows three plateaus: a glassy plateau (green), a rubber elasticity plateau (pink) and a high-temperature, low-frequency plateau (orange), referred to as sliding elasticity, wherein chain sliding and ring sliding occur simultaneously, a process that is not possible in covalent fixed-crosslinked networks. PEG, poly(ethylene glycol). Panels **a** and **b** reproduced with permission from REF.[114], SPSJ. Panel **d** adapted with permission from REF.[125], Elsevier B.V. Panel **e** adapted with permission from REF.[135], SPSJ.

Some authors even used a doubly threaded [3]rotaxane model to illustrate these concepts[110,111]. The sliding junction model introduced by Ito and colleagues[114,115] is conceptually similar to some of these theories: the free energy is minimized with respect to the distribution of monomers among several chains, leading to a lower Young's modulus than networks with fixed crosslinks. Furthermore, the lack of hysteresis in most SRMs is a consequence of the reversibility of the sliding motion of the rings.

Mechanical testing highlights the dramatic effect that a slide-ring crosslink can have on the properties of a polymer network. Small-amplitude oscillatory shear rheology[116] on SRGs of **9** in DMSO revealed a time-dependent stress relaxation modulus with two distinct plateaux at low frequencies: the first was attributed to the typical rubbery modulus, but the second (lower) plateau is not observed in networks with fixed crosslinks (FIG. 4e). These features have also been observed in step strain experiments on similar SRMs[117]. The rubbery plateau

implies a molecular weight between crosslinks, M_C, and the relaxation time, τ, associated with the transition between the two regimes scales as $\tau \sim M_C^3$ (REF.[116]). This dependence is the same as that predicted by reptation theory, which describes the sliding motion of a polymer chain[118], and, as a result, the researchers associated this 'sliding transition' with the sliding of the polymer chains through the ring crosslinks, accounting for the lower equilibrium modulus of figure-of-eight SRMs relative to fixed-crosslinked networks. However, the analogy with reptation theory may not be appropriate because there is no continuous confining tube in SRMs and the timescale for diffusion of tension along entangled chains actually scales as M_C^2 (REF.[118]). Thus, further study is required to clarify the dynamic processes responsible for the sliding transition. Nevertheless, it seems likely that ring sliding is responsible for the phenomenon in some fashion.

The impact of mobile crosslinks on material properties has also been investigated by molecular simulations[115,119–121]. These efforts demonstrate that the reduced modulus of SRMs is intimately related to the distance available for crosslink sliding, with greater freedom leading to softer materials[115,119]. Other in silico experiments have shown that SRMs exhibit excellent surface adsorption, because the stretchable networks can easily deform to maximize surface contact[121]. Further simulations showed that SRMs can rapidly absorb nanoparticles with diameters much larger than the network mesh size because the mobile crosslinks allow for efficient expansion of the network[121].

Given that mobility of crosslinks is a key factor in the properties of SRMs, the effective range of sliding strongly influences the behaviour, as suggested by the simulation studies discussed above. This range can be widened by increasing the molecular weight of the axis polymer, which results in improved fracture energy. However, increasing the crosslink density appears to mitigate some of these effects. For instance, small-angle neutron scattering and small-angle X-ray scattering experiments have shown that SRGs remain isotropic upon uniaxial deformation up to considerable strains and are homogenous even at large extensions, in contrast to networks with fixed crosslinks[99,122–124]. However, the structural inhomogeneities typical of these fixed networks emerge when the ring-sliding range is suppressed, either by increasing the crosslink density[117,122] or by using a solvent that favours ring aggregation[99].

The picture of SRMs discussed so far is incomplete; it does not explain why the second (low-frequency) plateau modulus has a finite, non-zero value. It also fails to address the unusually weak dependence of modulus, E, on crosslink density, ν, which seems to scale as $E \sim \nu^{0.2}$, rather than $E \sim \nu^1$ as expected for fixed-crosslinked networks[125], and is sometimes even non-monotonic[126]. Furthermore, in the simple picture illustrated above, SRGs at swelling equilibrium should display the same modulus as fixed-crosslinked gels. This observation was first made by de Gennes[127], who argued that the additional degrees of freedom afforded by mobile crosslinks would be entirely used to further swell the gel, rather than lower the modulus upon deformation. As a result, SRGs at equilibrium should be as stiff as fixed-crosslinked gels of comparable swelling and density of elastic strands. The discrepancy between this theoretical model and experimental results might be explained by the presence of uncrosslinked rings in experimental SRGs (pink rings, **9**).

The free rings along the polymer backbone possess translational entropy that can affect crosslink mobility. In particular, rings on a polyrotaxane backbone can be modelled as hard particles confined to 1D space. In this system, analogous to the Tonks gas in statistical mechanics[128], the configurational entropy of the rings gives rise to a pressure, which resists the motion of the crosslinks, as this reduces the contour length available to the molecules. The connection to polyrotaxanes was made by Sevick and Williams[129], who found that the presence of rings along the backbone (and the associated pressure) resists the sliding motion of the polymer chain through a fixed ring below a critical force, analogous to yield stress behaviour[130–134]. In the context of SRMs, the translational entropy of the uncrosslinked rings resists the sliding motion of the ring crosslinks, causing additional contributions to the elasticity, called 'sliding elasticity'[116,135].

Ito and colleagues have attempted to explain various properties of SRMs in qualitative terms by applying the concepts of sliding elasticity. For instance, they propose that the finite storage modulus of SRMs at long times cannot be understood purely in terms of crosslink mobility and the resistance to crosslink sliding caused by the uncrosslinked rings may furnish an explanation for this effect[116,135]. In addition, the Young's modulus can depend non-monotonically on crosslink density, increasing for small amounts of crosslinks and then decreasing at larger loadings; a model combining sliding crosslinks with the entropic effects of uncrosslinked rings can reproduce such an effect[126]. Ito and colleagues have also observed significant strain hardening upon compression of **9** (in DMSO), with the modulus transitioning from one constant value at low strains to another, higher value at intermediate strains[125]. The initial (smaller) and intermediate (larger) moduli agree quantitatively with the two plateaux observed in rheological measurements (FIG. 4e) . If these regimes do indeed reflect polymer and sliding elasticity, then one may conclude that the entropy of the rings dominates at small deformations and the entropy of the chains becomes more important at larger strains.

Despite the progress described above, the details of how ring entropy affects SRM mechanical properties are still unclear. Mobile rings on polyrotaxanes lead to yield stress behaviour, both in theory[131] and in simulation[136], but SRMs show no such effects. Moreover, if the low-frequency plateau in the viscoelastic data (FIG. 4e) is associated with crosslink sliding, then the average force on each network strand must be greater than the yield force. However, the expected yield force appears to be quite large compared with the stresses observed in linear viscoelasticity measurements[116,131]. In general, it is unclear how the microscopic properties of polyrotaxanes with mobile rings connect to the macroscopic properties of SRMs. Molecular simulations of model systems, such as those by Müller et al.[136], may prove useful in resolving these questions.

Structure–property relationships in SRMs. As discussed above, the mobility of the figure-of-eight rings in SRM **9** influences its material properties. However, a range of factors impact this mobility, including the distance available for ring sliding, crosslink density, ring size and ring–thread interactions. As such, understanding the complex relationship between these factors is important for creating a structure–property profile of these intriguing materials.

The ring coverage of a polyrotaxane is defined as the percentage of polymer backbone covered by the rings. Reducing the coverage increases the sliding distance between rings and, therefore, increases the crosslink mobility. This relationship was demonstrated by studying the mechanical properties of two related SRGs (**10**) with different ring coverages (2%: **10-02**, FIG. 5a top, and 25%: **10-25**, FIG. 5a bottom) but similar degrees of crosslinking[102]. The 25 wt% **10-02** hydrogel exhibited excellent extensibility (up to 1,600%) and was capable of reaching over 1.1 MPa stress-at-break, while, for comparison, fixed-crosslinked gels with similar elasticity usually exhibited <10 kPa stress-at-break. Fatigue performance of **10-02** was determined via successive cyclic tensile tests, which showed that stretching the material to seven times its original length (extension ratio, $\lambda = 7$) for 100 cycles resulted in stress–strain curves that nearly overlap. Additionally, loading–unloading cyclic tensile tests on **10-02** showed almost no hysteresis during the first three cycles at low extension, and only 3% residual strain during the fourth cycle ($\lambda = 12$, FIG. 5b).

Comparison between the SRGs of different ring coverage was carried out with the 16 wt% hydrogels. Tensile studies showed that the lower coverage **10-02** exhibited vastly superior strain and stress-at-break relative to the higher coverage **10-25** (1,250% strain, 125 kPa stress versus 110% strain, 50 kPa stress, respectively). A similar effect has been observed in SRGs (with DMSO solvent) prepared from related polyrotaxanes[137], as well as slide-ring hydrogels[117] and non-figure-of-eight SRGs[138]. These observations are consistent with the larger number of uncrosslinked rings limiting mobility, resulting in inferior mechanical properties.

Reducing ring coverage on polyrotaxane chains within SRMs also improves their fracture toughness. Notched samples of **10-02** (16 wt%) had a critical strain of crack propagation three times that of **10-25** (FIG. 5c, left), although both samples showed better fracture toughness than an equivalent fixed-crosslinked gel[105,139]. Plane polarized-light images (FIG. 5c, right) of these stretched materials showed remarkable differences in the stress relaxation mechanism; **10-02** appears to undergo homogenous distribution of stresses throughout the material, whereas a butterfly-shaped pattern is observed in **10-25**, consistent with heterogeneous distribution of stress. Furthermore, crack propagation occurred 40 times slower in the lower coverage SRMs[105]. From a molecular perspective, these observations are consistent with lower ring coverage allowing greater freedom of movement of the slide-ring crosslinks and, therefore, more efficient stress relaxation.

The range of ring motion along polymer chains will also be impacted by the number (or density) of sliding crosslinks. In fixed-crosslinked networks, increasing the covalent crosslink density leads to a higher modulus, reduced strain-at-break, lower toughness and lower swelling. The same qualitative trends are typically observed in SRMs when the sliding-crosslink density is increased. However, the situation is more complicated because there are two forms of entropic elasticity, namely, from the polymer chains and ring sliding. As a result, SRMs do not exhibit a linear relationship between crosslink density and elastic modulus, as is expected for fixed-crosslinked networks. How the SRM mechanical properties are affected by changing the crosslink density can depend on the ring coverage of their polyrotaxane precursors. For example, SRMs with higher ring coverage (~25%) can show non-monotonic changes in elastic modulus as the crosslinking density is varied, first increasing at small densities (up to about 1.0–1.5%) and then decreasing at higher values[126,137]. However, this behaviour is not observed in all circumstances, suggesting a more complex relationship[102]. Such non-monotonic behaviour is generally not seen in low-coverage figure-of-eight SRMs, or in other SRM architectures[140,141]. Other factors such as microphase separation can also complicate the relationship between modulus and crosslink density[142]. One feature observed in most SRMs is that the Young's modulus scales slowly with crosslink density, having an exponent well below unity, in contrast to the linear scaling of networks with fixed crosslinks. This weak dependence suggests that chain entropy does not contribute as strongly to the elasticity of SRMs as ring entropy.

Understanding network elasticity can be difficult, even in fixed-crosslinked networks, because defects, such as loops and dangling ends, must be accounted for. SRMs present additional challenges because intramolecular reactions between CD rings on the same polyrotaxane chain can lead to the formation of 'tubes'[143,144] (as in **9**, FIG. 5d, left), which increase polymer segment stiffness and, therefore, modulus. These confounding factors make it difficult to build a comprehensive understanding of the relationship between crosslink density and mechanical response. Ito and colleagues[101] addressed some of these issues by crosslinking alkyne-functionalized and azide-functionalized polyrotaxanes (**11**$_{alk}$ and **11**$_{az}$) to form SRM **12** (FIG. 5d, centre), thereby, eliminating tube formation. This approach also reduces loop formation because single-chain loops are not possible[101]. Furthermore, the resulting triazole crosslinks can be detected by UV spectroscopy, providing an accurate estimate of crosslink density.

The modulus of these specially designed SRGs (in DMSO) exhibited a very weak dependence on crosslink density, $E \propto \nu^{0.5}$ (FIG. 5d right, red data points, compared with $E \propto \nu$ for fixed-crosslinked networks). As discussed above, the relationship between modulus and crosslink density is also affected by ring coverage; for instance, **12-05** made from 5% coverage polyrotaxanes (**11-05**$_{az}$ and **11-05**$_{alk}$) exhibit a lower modulus than **12-25**, although the dependence on crosslink density appears to be stronger (FIG. 5d right, blue data points). However, the range of synthetically accessible crosslink densities for **12-05** is narrow, so the precise relationship between

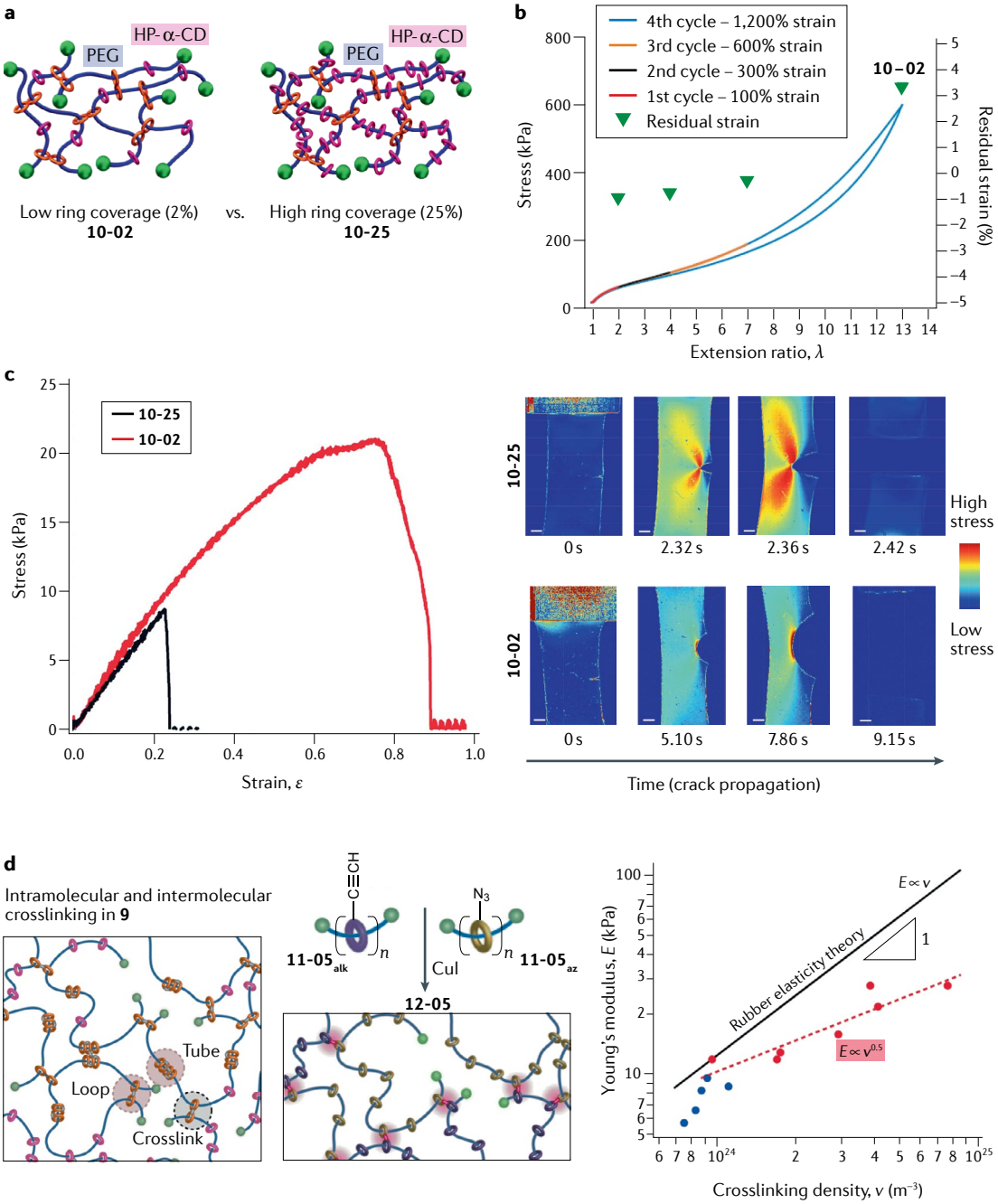

Fig. 5 | **Structure–property relationships in slide-ring materials. a** | Schematic of the figure-of-eight **10-02** and **10-25** hydrogels that consist of poly(ethylene glycol) (PEG) backbones and partially functionalized hydroxypropyl-α-cyclodextrin (HP-α-CD), with similar crosslink density but different ring coverage: 2% (left) and 25% (right). **b** | Loading–unloading cyclic tensile tests on **10-02** (25 wt% hydrogel) at different strains, with the residual strain after each cycle revealing little to no hysteresis at lower extensions and small residual strain during the fourth cycle (1,200% strain, $\lambda = 12$). **c** | Fracture tensile properties of notched 16 wt% hydrogel samples of **10-02** and **10-25**; the critical strain of crack propagation of **10-02** is three times that of **10-25** (left). Polarized-light images of notched samples of the same materials mapping localized stresses throughout the material (warmer colours represent greater stress); a highly blunted notched region is observed in **10-02**, in addition to a smaller area of high stress (red) relative to **10-25** (right). **d** | Intermolecular crosslinking of chemically identical polyrotaxanes (for example, **1**) yields slide-ring materials that contain 'loops' and 'tubes' as a result of unintended intramolecular crosslinking, as shown in **9**. Complementary functionalities (azide (yellow) and alkyne (purple)) on the polyrotaxane α-CDs of $\mathbf{11\text{-}05}_{az}$ and $\mathbf{11\text{-}05}_{alk}$ prevent intramolecular reactions during crosslinking forming **12-05** (centre). Correlation between modulus, E, and crosslink density, ν, for **12-25** ($E \propto \nu^{0.5}$, red data points), showing a deviation from rubber elasticity theory ($E \propto \nu$); blue data points correspond to **12-05** (right). Panel **b** reprinted with permission from REF.[102], ACS. Panel **c** reprinted with permission from REF.[105], IOP Publishing. Panel **d** reprinted with permission from REF.[101], ACS.

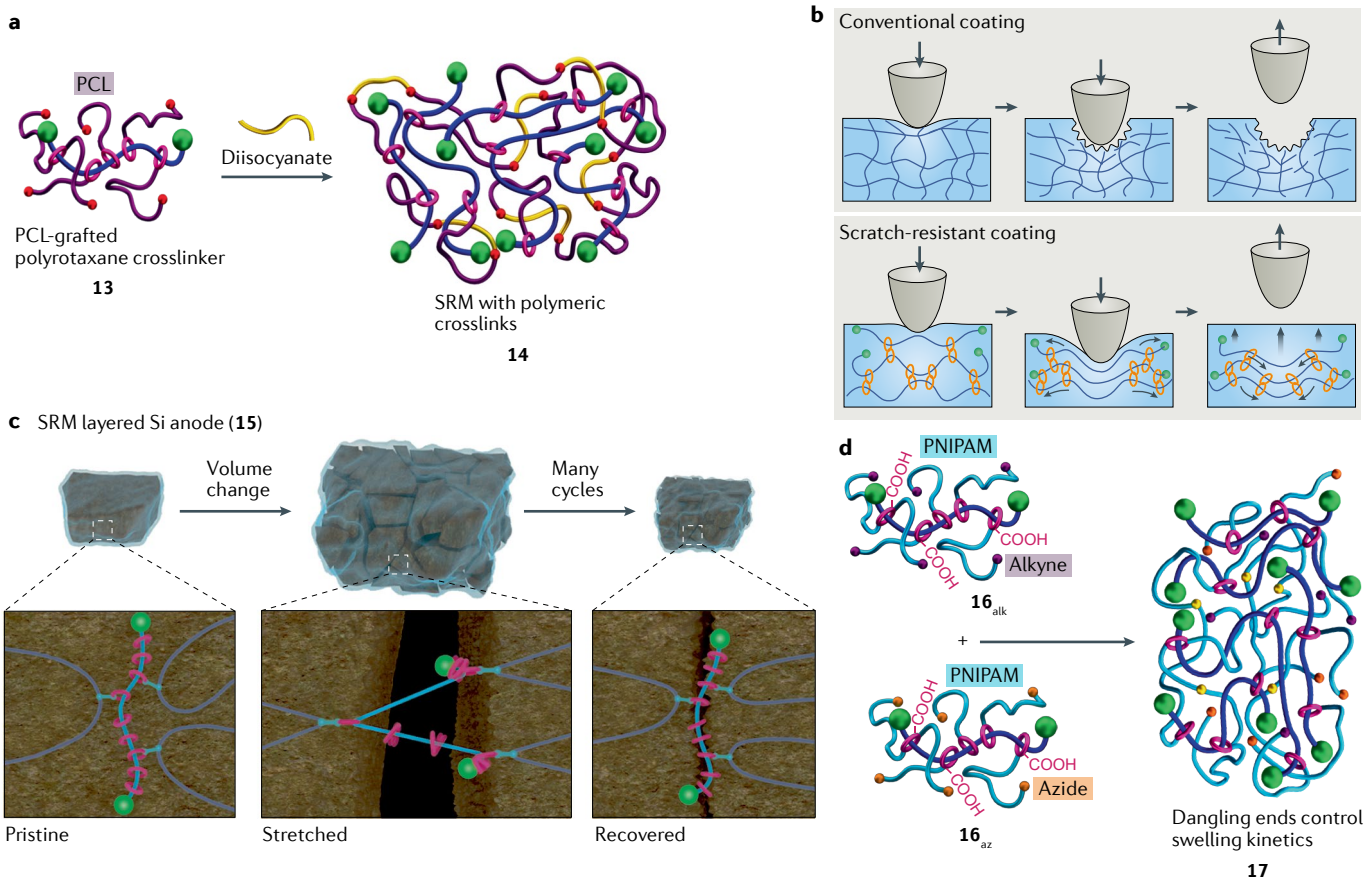

Fig. 6 | **Engineering slide-ring materials for targeted applications.** **a** | Grafting of polycaprolactone (PCL, purple) from the cyclodextrins of **2** yields the PCL-grafted polyrotaxane (**13**) with hydroxyl chain ends (red) that can be crosslinked with a diisocyanate (yellow) (dibutyltin dilaurate (cat.)) to access the slide-ring material (SRM), **14**. **b** | Cartoon showing deformation of a conventional coating and a slide-ring coating; the latter exhibits physical healing. **c** | Graphical representation of the proposed stress dissipation mechanism in a silicon (Si) anode layered with **15** (which comprises **2** and poly(acrylic acid)) during the charge–discharge cycles of a Li-ion battery. **d** | Poly(*N*-isopropylacrylamide) (PNIPAM)-grafted, carboxylated-cyclodextrin polyrotaxanes with alkyne (purple, $\mathbf{16}_{alk}$) and azide (orange, $\mathbf{16}_{az}$) chain ends that crosslink (yellow) to form **17** with varying amounts of dangling PNIPAM chain ends. Panel **b** reprinted with permission from REF.[151], Wiley Periodicals, Inc. Panel **c** reprinted with permission from REF.[160], AAAS.

E and *v* for lower-coverage SRMs is not fully established at this time.

Molecular dynamics simulations have shown that increasing ring size in polyrotaxanes can lead to faster ring diffusion (or reduced friction) along the backbone[33]. As a result, the size of the ring component is expected to have a significant impact on the dynamical properties of SRMs. While SRGs have been synthesized and studied with various ring sizes (for example, α-CD compared with γ-CD)[104], solvent effects complicate the results and make them difficult to interpret. Taking a different approach, Takata and colleagues[145] investigated this concept using non-figure-of-eight rotaxane-crosslinked networks. Rather than change the diameter of the rings, they altered the width of the thread by using a polyrotaxane backbone with different alkyl substituents. Although the thicker-thread SRMs have the same strain-at-break as those with thinner threads, their fracture stress (and energy) are actually larger. This suggests that greater force is required to pull the rings along thicker backbones, consistent with the idea that 'friction' associated with ring sliding is increased for thicker threads, smaller rings or a combination of both.

SRM architectures beyond the figure-of-eight. As discussed at the end of the previous section, researchers have investigated SRM architectures beyond the original figure-of-eight gels. In this prior example, multiple polymerizable groups are installed on the polyrotaxane rings or stoppers, which allows the polyrotaxanes to act as crosslinkers for copolymerization or direct reaction with other polymers[138,146–148]. This approach has been used to synthesize SRMs with both covalent and sliding crosslinks[147,149,150], so that material properties can be tuned smoothly between the fully topological and fully covalent limits.

An alternative SRM architecture can be prepared by grafting polymer chains onto the rings of a polyrotaxane and crosslinking through the chain ends[141]. By varying the polymers used as grafting chains, it is possible to introduce new chemistries and tailor material properties. For example, polyrotaxane **2** (REF.[97]) grafted with polycaprolactone (PCL) (**13**, FIG. 6a) is commercially available and can be used as a crosslinker to form SRM **14** upon reaction of the grafted polymer chain ends with other monomers. On account of its excellent stress recovery, a highly crosslinked, low-T_g SRM **14** has

been commercialized as a UV-curable, scratch-resistant coating for automobiles and electronic devices[151]. When a scratching force is applied to these SRMs, the rings are able to slide away and then recover when the force is released, resulting in physical self-healing of the scratch (FIG. 6b).

Using either of these strategies, sliding crosslinks have been incorporated in polylactones[141,152], polylactide[142], acrylates[148,153] and polyurethanes[154], to name a few. In general, the addition of sliding crosslinks leads to lower (or similar) elastic modulus, higher extensibility, improved toughness and greater swelling relative to comparable materials with fixed crosslinks. Furthermore, the effects of changing ring coverage, crosslink density and ring size discussed in the previous sections typically remain valid in these materials. Note, however, that some of these systems do not possess uncrosslinked rings as in the figure-of-eight systems, so the 'sliding elasticity' described above is not always relevant.

Finally, it is noteworthy that there is an ever-expanding library of distinct SRM architectures being developed that continues to investigate how topological crosslinking can be used to enhance material properties. For example, oligomacrocyclic species have been used to form SRMs, typically with the goal of creating recyclable or degradable materials[155–157].

Engineering SRMs towards applications. Polyrotaxanes based on CD and PEG are commercially available[151], leading to an increase in studies aimed at engineering SRMs towards applications. The discussion below highlights areas in which SRMs have attracted attention. However, the potential of SRMs goes beyond these areas, reaching fields as diverse as vibration-proof and sound-proof insulation materials[151], ion transport[158] and icephobicity[159].

As discussed above, SRMs have allowed access to coatings that self-heal a scratch and this resiliency has made SRMs useful in other applications. For example, in Li-ion batteries with polymer-bound Si particle anodes, the particles experience large volume changes during charge–discharge cycles, leading to particle degradation and limited battery lifetime[160,161]. Stress from the volume changes can be mitigated with the use of a SRM as the anode binder (FIG. 6c). For example, SRM **15** is prepared by the reaction of **2** (5 wt%) with a conventional polymer binder, polyacrylic acid, resulting in a substantial improvement of the mechanical properties. As a result, the use of **15** as a binder for the anode yielded a 91% capacity retention after 150 cycles, whereas the anode with a more standard polyacrylic acid binder attained only 48% of its original capacity after 50 cycles. It was proposed that the interlocked crosslinks slide and equalize stress to cushion the silicon microparticles during charge–discharge cycles.

Dynamic covalent chemistry[162] has been introduced into SRMs to provide an additional mechanism for healing. For instance, boronic acid and diol moieties have been attached to CD rings to access interlocked dynamic polyrotaxane crosslinkers[163]. This combination of sliding crosslinks and dynamic bonds results in SRMs capable of self-healing with greater efficiency than non-sliding dynamic covalent networks, making them excellent candidates for scratch-resistant coatings. Similarly, combining sliding crosslinks with carboxyl-Fe^{3+} coordination yields tough and highly recoverably metallosupramolecular hydrogels[164].

Stimuli-responsive hydrogels have garnered interest in a number of fields, including drug delivery, biosensing and artificial muscles[165–167]. Sliding crosslinks hold great promise for improving the properties of existing stimuli-responsive hydrogels, particularly those that undergo large or rapid volume changes that cause stress concentrations in fixed-crosslinked networks. For example, α-CDs functionalized with photoresponsive azobenzene moieties provide access to SRMs with large photoinduced swelling–deswelling[168]. The sliding crosslinks distribute stresses evenly throughout the network, leading to more robust materials with longer lifetimes.

Polymers with a lower critical solution temperature are commonly used in stimuli-responsive hydrogel research, with poly(*N*-isopropylacrylamide) (PNIPAM) being the most widely studied[169]. However, these fixed-crosslinked hydrogels often become brittle or lose transparency upon repeated swelling and deswelling. As such, it is not surprising that polyrotaxanes have been incorporated into PNIPAM networks[170–172] and other polyacrylamides[173,174] to improve toughness, swelling capacity, optical properties and material lifetime. In general, the better-performing materials used polyrotaxane **2** crosslinkers with carboxylated rings, where the ionic groups enhance water-solubility and uptake.

Building on such studies, it has been shown that the shrinking rate of PNIPAM-based SRMs can be tuned by varying the amount of 'dangling chains' attached to the CD rings. In particular, Takeoka and colleagues[175] prepared polyrotaxanes in which alkyne or azide end-capped PNIPAM chain grafts were present on rings of carboxylated polyrotaxane **2** (**16**$_{alk}$ and **16**$_{az}$, FIG. 6d). Subsequent crosslinking of **16**$_{alk}$ and **16**$_{az}$ via click reaction yields SRM **17**, where the ratio of crosslinked to dangling chains was controlled by varying the reaction time. Increasing the amount of dangling chains from 39% to 46% increased the equilibrium swelling ratio and accelerated the shrinking rate. It was suggested that the ring mobility allows the thermoresponsive dangling ends to distribute themselves evenly throughout the network, improving the material response.

Slide-ring material resins. Highly crosslinked, high-T_g resins are the oldest synthetic commercial polymers produced and are still commonly used today as structural, impact-resistant or adhesive materials. Unfortunately, these materials are often brittle, trading toughness for high modulus. However, by incorporating slide-ring crosslinks into the materials, both modulus and toughness can be improved. For example, Seo and colleagues[176] incorporated polyrotaxane **1** into a commonly used epoxy resin. Here, the α-CD hydroxy groups act as nucleophiles during the curing reaction, resulting in a material that has both covalent and sliding crosslinks. Given that each α-CD possesses 18 hydroxy groups, the resulting SRMs have higher crosslinking density than

the original material, which leads to greater stiffness and tensile strength. However, despite the stiffness of the surrounding matrix, the PEG chains of the polyrotaxane are still able to slide through the CDs, allowing the material to relieve internal stresses[177]. Such polymer chain mobility has also been observed in polyrotaxane glasses[29] and leads to greater strains-at-break and toughness.

The mechanical properties of SRM resins can be tuned by controlling the amount of topological crosslinking by modifying the α-CDs in **1**. For instance, tertiary amines installed on the polyrotaxanes accelerate resin formation while limiting the number of hydroxy groups available for crosslinking. As a result, the crosslink density is increased when an average of one tertiary amine per CD is used, but decreased when a CD with an average of four tertiary amines per CD is used[176]. All SRM resins showed improved toughness compared with the fixed-crosslinked epoxy, and this toughness increased concomitantly with crosslink density and stiffness, in contrast to conventional resins and unlike the lightly crosslinked, low-T_g SRMs discussed above[178]. Similar enhancements in toughness can be achieved by incorporating polyrotaxane **1** as a crosslinker into other high-T_g resins[179–181], in addition to improvements in adhesive strength[182]. In each case, the higher extensibility of the materials is attributed to the additional mobility of the slide-ring crosslinks in the network.

Molecular daisy chains

Another class of rotaxane-based MIPs are the daisy-chain polymers, which have the mechanical bond as an intrinsic part of the polymer backbone. An archetypical version of this class of MIP is the poly[2]rotaxane (FIG. 2a top right), and, although there are several reports on the synthesis of this class of polyrotaxane, the reporting of material properties has been limited[93,183–185]. A more studied subset of daisy-chain polymers are those that incorporate a dimeric cyclic daisy chain ([*c*2]daisy chain) as the mechanical bond. In this class of MIPs, the dimeric [*c*2] daisy-chain interlocked motif allows components to slide past each other and enables access to either contracted or expanded forms[186,187] (FIG. 1d). Thus, the incorporation of such linkages into a polymer offers a route to actuating or switchable materials that can undergo macroscopic changes based on molecular motion.

Strides towards linear [c2]daisy-chain-containing polymers were made by Grubbs, Stoddart and colleagues[188–191], who polymerized bifunctional [*c*2]daisy-chain monomers using either azide–alkyne cycloaddition or alkene metathesis chemistry. The resulting polymers (FIG. 7a) could be switched between contracted (**18-H**$^+$) and expanded (**18**) forms by changing the pH of the solution. Subsequent efforts have focused on the design of network materials (either supramolecular[192–197] or covalent[198–200]) aimed at exploiting this molecular actuation in material systems. As an example, network [*c*2] daisy-chain (based on crown ether-ammonium recognition sites) gels[198] in acetonitrile have been developed to allow switchable swelling–deswelling behaviour with the addition of acid or base.

UV-switchable [*c*2]daisy-chain networks (**19**) have been prepared by reacting a four-armed PEG linker with a bifunctional [*c*2]daisy-chain monomer, comprising an α-CD and stilbene[200] (FIG. 7b, left). The photoresponsive stilbene is known to bind stronger with α-CD in its *trans* conformation. Switching between **19-*trans*** and **19-*cis***, which can be achieved by irradiation, results in the contraction ($\lambda = 350$ nm) or expansion ($\lambda = 290$ nm) of the network. This relatively rapid and robust photoswitching can result in UV-induced macroscopic bending of films by unidirectional irradiation of the material (FIG. 7b, right), and such films have been shown to lift objects 15 times their own weight[200]. Related photoresponsive [*c*2] daisy-chain networks that use azobenzene rather than stilbene have also been reported[199].

Polycatenanes

The mechanical bond in a catenane is able to undergo several modes of motion, including elongation, ring twisting and ring rotation (FIG. 1e), and these motions have the potential to influence the properties of a polymeric material. While there are a number of different ways to incorporate catenanes into a polymer architecture, perhaps the most impactful is within the polymer backbone or crosslinking units. FIGURE 8a shows a selection of such polycatenanes, which include poly[2]catenanes (FIG. 8a, top left), polymeric [2]catenanes (FIG. 8a, top right), poly[*n*]catenanes (akin to a macroscopic chain) (FIG. 8a, bottom left) and Olympic gels (or network catenanes, FIG. 8a, bottom right).

By its very nature, the catenane synthesis must include a ring-closing step, a process that is generally not as high yielding as the stoppering reaction frequently employed in (poly)rotaxane synthesis. These lower yields often hinder the formation of catenane-containing polymers on the scale necessary to fully study their thermophysical properties. As a result, theoretical and computational studies have been more influential in characterizing the material properties of such systems. Nonetheless, over the years, a wide range of polycatenanes have been prepared and, while our understanding of this class of MIPs is not at the level of the polyrotaxanes and SRMs, there are studies that point to the potential of polymers that contain interlocked rings.

Poly[2]catenane

Early polycatenane syntheses employed the polymerization of appropriately functionalized [2]catenane monomers to yield poly[2]catenanes[18] (FIG. 8a). Several reports of this architecture used a functionalized [2] catenane (**20**) (REFS[201–203]) (FIG. 8b). Early studies focused on $\mathbf{20_H}$ ($R_1 = H$); however, the inter-ring hydrogen bonding (between the N–H of one ring and the O=C of the other) hindered ring mobility. In addition, the $\mathbf{20_H}$ had limited solubility, so poly[2]catenanes were prepared using the methylated catenane $\mathbf{20_{Me}}$ ($R_1 = Me$). The bisphenolic $\mathbf{20_{Me}}$ was reacted with a diacid to yield $\mathbf{21_{Me}}$ with a number average degree of polymerization (DP_n) of 14 (FIG. 8b). Unfortunately, the bulky methyl groups within the rings hindered mobility of the [2] catenane units. A related [2]catenane (**22**, FIG. 8c) was able to overcome the solubility and ring-mobility obstacles of **20**. In **22**, the ring (**23**) is now large enough that the components are able to freely rotate when the

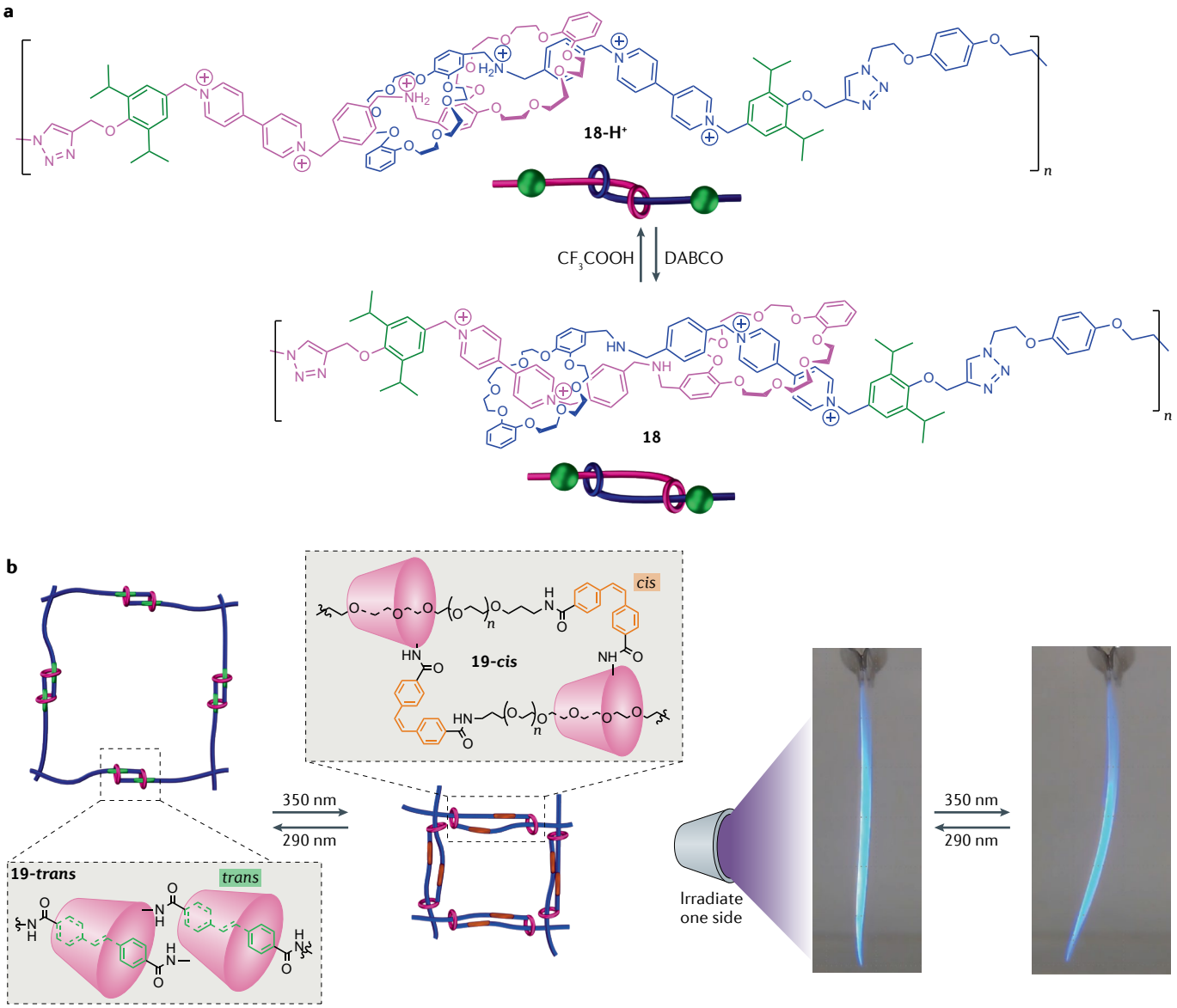

Fig. 7 | **[c2]Daisy-chain polymers. a** | Structure of an acid–base switchable linear [c2]daisy-chain polymer, polymerized by alkyne–azide cycloaddition. Protonation of the secondary amines in **18** to yield **18-H⁺** results in contraction of the polymer backbone, while deprotonation of the acidic form via addition of base (1,4-diazabicyclo[2.2.2]octane (DABCO)) reverts the polymer back to its expanded form. **b** | Stilbene-containing [c2] daisy-chain network polymer (**19**), where the position of the α-cyclodextrin rings can be directed using ultraviolet light. *Trans*-stilbene binds strongly to the α-cyclodextrin rings, locking them in place. Irradiation with 350-nm light induces *trans–cis* isomerization, resulting in weaker binding and movement of the rings along the poly(ethylene glycol) backbone, causing the network structure to contract. The expanded structure can be recovered upon *cis–trans* isomerization of the stilbene moiety with 290-nm light (left). The hydrogel was hung with a clip and irradiated with ultraviolet light on one side. When irradiated with 350-nm light, there is an anisotropic response of the material as the hydrogel exposed to light contracts, causing a bending motion. The original shape is obtained by irradiation at 290 nm (right). Panel **b** adapted and reprinted with permission from REF.[200], ACS.

nitrogens are methylated (**22**$_{Me}$), while hydrogen bonding in the unmodified version (**22**$_{H}$) renders the rings immobile[204–208] (FIG. 8c).

22$_{Me}$ was incorporated into a bisphenol A polycarbonate (BPAPC) backbone at 10, 20 and 30 wt% (FIG. 8c bottom, (**BPA-*r*-22**$_{Me}$) (10–30 wt%))[204,205]. In BPAPC, two thermal transitions are typically observed at −100 °C and 80 °C via dynamic mechanical analysis. While the same transitions are observed in (**BPA-*r*-22**$_{Me}$) (20 wt%), a new sub-T_g thermal transition is observed at −6 °C that was attributed to large conformational changes in the catenane segments, for instance, alkyl chain rearrangement or partial ring rotation.

The above study suggests that catenanes within a polymer backbone can elicit effects on the polymer's thermal behaviour. However, it has also been shown that the presence of just a single catenane in the polymer chain can impact its overall properties. This was shown with **PEO-22-PEO** (FIG. 8c, bottom), in which a PEO (M_n = 2,000 g mol^{-1}) chain was attached to each ring of a single molecule of **22** (though structurally different than the above examples, this system has also been

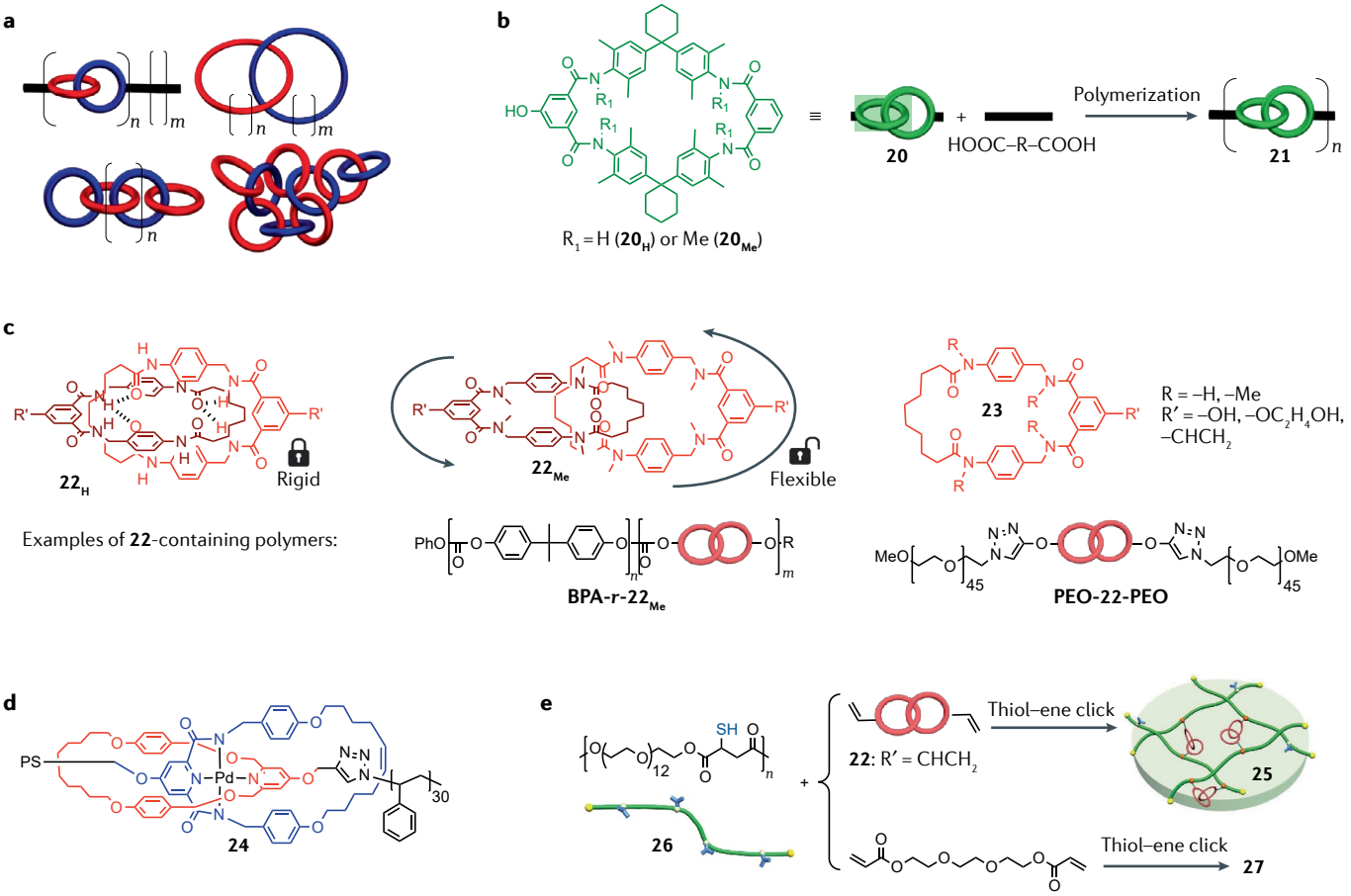

Fig. 8 | **Poly[2]catenane materials. a** | Various polycatenane architectures: a poly[2]catenane (top left), a polymeric [2]catenane (top right), a poly[*n*]catenane (bottom left) and an Olympic gel (bottom right). **b** | Catenanes $\mathbf{20_H}$ and $\mathbf{20_{Me}}$ can be polymerized via esterification to access poly[2]catenanes ($\mathbf{21_H}$ and $\mathbf{21_{Me}}$, respectively). **c** | The [2]catenane monomer ($\mathbf{22_H}$), which consists of two interlocked **23** rings, has a locked rigid conformation on account of hydrogen bonding between its rings (top left), while $\mathbf{22_{Me}}$ has four methylated nitrogens and is more flexible and mobile (top centre). A selection of polymers created with **22** is shown. **d** | A [2]catenane with Pd locking capability is used to create **24**. **e** | The synthesis of the catenated network **25** and the related fixed covalent network **27**. **f** | Temperature sweep rheology for the interlocked (**25**) and fixed-crosslinked (**27**) acetonitrile gels showing softening of $\mathbf{25_H}$ upon protonation ($\mathbf{25_H}$-$\mathbf{H^+}$) (left) (G′, shear storage modulus; G″, shear loss modulus). Stress–strain curves for acetonitrile gels $\mathbf{25_H}$ (centre) and $\mathbf{25_{Me}}$ (right) in neutral and acidic conditions. BPA, bisphenol A; PEO, poly(ethylene oxide); PS, polystyrene. Panels **e** and **f** reprinted with permission from REF.[208], Wiley-VCH.

referred to as a poly[2]catenane)[207]. Similar to the studies discussed above, both freely jointed (**PEO-$\mathbf{22_{Me}}$-PEO**) and locked (**PEO-$\mathbf{22_H}$-PEO**) polymers have been investigated. Force-extension experiments have shown that the freely jointed **PEO-$\mathbf{22_{Me}}$-PEO** had a smaller persistence length (0.45 ± 0.05 nm) than the locked **PEO-$\mathbf{22_H}$-PEO** (1.0 ± 0.15 nm), suggesting that the presence of a single mobile mechanical bond is enough to significantly enhance the chain mobility. Related MIPs have been investigated with high-T_g polymers attached to a [2]catenane. For example, a single molecule of catenane $\mathbf{24_{Pd}}$ (prepared via Pd(II) templating) was grafted with polystyrene (M_n = 3,100 g mol^{-1}) to access **PS-$\mathbf{24_{Pd}}$-PS**[209] (FIG. 8d). The polymer with the immobile metal-bound catenane (**PS-$\mathbf{23_{Pd}}$-PS**) has a T_g of 120 °C. However, the metal-free, more mobile **PS-24-PS** has a T_g of 109 °C, only 2 °C above neat polystyrene of a similar molecular weight. This result suggests that the motion of the

catenane is able to offset the physical disruption caused by the bulky catenane rings.

[2]Catenanes have also been incorporated into polymer networks. For example, catenane **22**-containing hydrogels ($\mathbf{25_{Me}}$ and $\mathbf{25_{H}}$) have been prepared by reacting a thiol-containing polyester (**26**, $M_w = 9{,}100\ g\ mol^{-1}$) with the mobile catenane $\mathbf{22_{Me}}$ or the hydrogen-bonded catenane $\mathbf{22_{H}}$ (REFS[208,210,211]) (FIG. 8e). **26** was also reacted with a PEG diacrylate to create a control covalently crosslinked hydrogel (**27**). Rheological data (FIG. 8f, left) of $\mathbf{25_{H}}$ and $\mathbf{25_{Me}}$ show that the hydrogel $\mathbf{25_{H}}$ is stiffer at ambient conditions as a consequence of the less mobile [2]catenane. In addition, the modulus of $\mathbf{25_{H}}$ is reduced at high temperature as the $\mathbf{25_{H}}$ hydrogen bonds are disrupted. In contrast, $\mathbf{25_{Me}}$ is softer at room temperature and shows little temperature sensitivity, as there are no hydrogen bonds to disrupt. In a similar vein, the hydrogen bonding in $\mathbf{22_{H}}$ can be disrupted by the addition of acid. As such, $\mathbf{25_{H}}$ is pH-responsive, with the $\mathbf{25_{H}}$-$\mathbf{H^{+}}$ exhibiting moduli similar to that of $\mathbf{25_{Me}}$. In contrast, no pH-sensitive behaviour was observed in $\mathbf{25_{Me}}$ nor the control **27**. This pH-switching characteristic also affects the stress–strain behaviour of the gels (FIG. 8f, centre and right): the gels with the mobile catenanes, $\mathbf{25_{Me}}$ and $\mathbf{25_{H}}$-$\mathbf{H^{+}}$, were softer and more extensible, while the gel with the immobile rings ($\mathbf{25_{H}}$) possessed a larger elastic modulus and smaller strain-at-break. This work demonstrates that the mechanical properties of these materials are impacted by the mobility of the catenanes and shows that mobility of [2]catenanes can be leveraged to create stimuli-responsive materials.

Polymeric [2]catenanes

Not to be confused with poly[2]catenanes, a polymeric [2]catenane consists of two cyclic polymers interlocked with a single mechanical bond (FIG. 8a, top right). Early synthesis of polymeric [2]catenanes focused on the use of statistical threading[212], which was low yielding and the resulting catenanes had to be painstakingly separated from linear and non-catenated cyclic polymers. Recent efforts have focused on templating strategies that are higher yielding[213–216] and improved methods of purification[217].

The most extensive materials characterization of polymeric [2]catenanes to date are studies performed by Advincula and colleagues. In particular, catenated PCL was synthesized via ring expansion to yield two interlocked cyclic polymers ($M_n = 12{,}000\ g\ mol^{-1}$ or $22{,}000\ g\ mol^{-1}$ for the MIPs). Both polymeric [2]catenane materials and their linear PCL counterparts of similar molecular weight ($M_n = 11{,}000\ g\ mol^{-1}$ and $21{,}000\ g\ mol^{-1}$) were subjected to differential scanning calorimetry heating and cooling cycles to assess how catenation affects crystallinity. The two catenated materials demonstrated lower degrees of crystallinity (42% and 49%) than the corresponding linear PCL samples (52% and 57%), which was attributed to the self-constrained architecture present in the catenanes that limits the mobility of the polymer chains. In addition, wide-angle X-ray scattering studies showed that PCL formed more compact crystalline structures than the interlocked polymers, again, presumably resulting from the permanent entanglements in the MIP[215].

Poly[n]catenane

Poly[*n*]catenanes consist entirely of interlocked rings (FIG. 8a, bottom left) and researchers have, in the past, speculated that these polymers could exhibit a large loss modulus, rapid stress relaxation and low activation energy for flow[218,219]. It is worthwhile pointing out that there is little theoretical basis for these conjectures and the theoretical works[220,221] that are sometimes cited as evidence for these properties do not address rheology; however, it is, nevertheless, reasonable to assume that the large number of interlocking components in these polymers will indeed impart unique or unusual properties on these materials. Unfortunately, the synthesis of such polymers is still a major challenge that has inhibited detailed evaluation of their properties.

Historically, the synthesis of [5] and [7]catenanes had been performed in a stepwise approach, where rings were added in a consecutive manner[222–224]. Although these syntheses were major achievements in MIM research, this approach is not amenable to the synthesis of long polymers, because the number of steps required to achieve even moderate degrees of polymerization is prohibitive. A different approach[225] sought to create a poly[2]catenane with cleavable bridged linkers. Cleavage of the covalent bridges would result in the formation of expanded rings, yielding the desired poly[*n*]catenane. Although bridged poly[2]catenanes and oligo[2]catenanes were successfully synthesized, a poly[*n*]catenane has not be prepared by this method to date.

More recently, relatively long chain poly[*n*]catenanes have been synthesized using a metallosupramolecular polymer template and ring-closing metathesis[219] (FIG. 9a, **28**). Analysis of the interlocked products (obtained in ca. 70–80% yield) showed a mixture of linear, cyclic and branched poly[*n*]catenanes with an average molecular weight (M_n) of $21{,}400\ g\ mol^{-1}$, corresponding to a DP_n of 14 (FIG. 9b). To isolate the various architectures and sizes, **28** underwent size exclusion chromatography and the individual fractions were analysed separately. In the largest M_n fraction, highly branched poly[*n*]catenanes with up to 130 rings were observed, with an average DP_n of 55. The smaller M_n fractions contained primarily linear and cyclic poly[*n*]catenanes, with an average DP_n of 12 and 8, respectively.

Poly[*n*]catenane **28** possesses metalloresponsive behaviour as a direct consequence of the metal templating used in the synthesis. Although the rings are free to rotate when demetalated, they are locked when in the presence of metals, which reform the metal–ligand complex in the polymer. The locked arrangement causes large changes in T_g and polymer size. For instance, in linear poly[*n*]catenanes, an increase of T_g from 97 °C to >160 °C was observed upon metalation with Zn^{2+}. In solution, the same polymers exhibited a 70% increase in hydrodynamic radius (from 3.9 nm to 6.6 nm) upon metalation, consistent with a less flexible structure in the presence of Zn^{2+}.

As poly[*n*]catenane synthesis is still highly challenging, molecular simulations are currently the most productive tool for studying these systems. Over the past two decades, a number of theoretical and computational studies have examined idealized poly[*n*]catenanes either

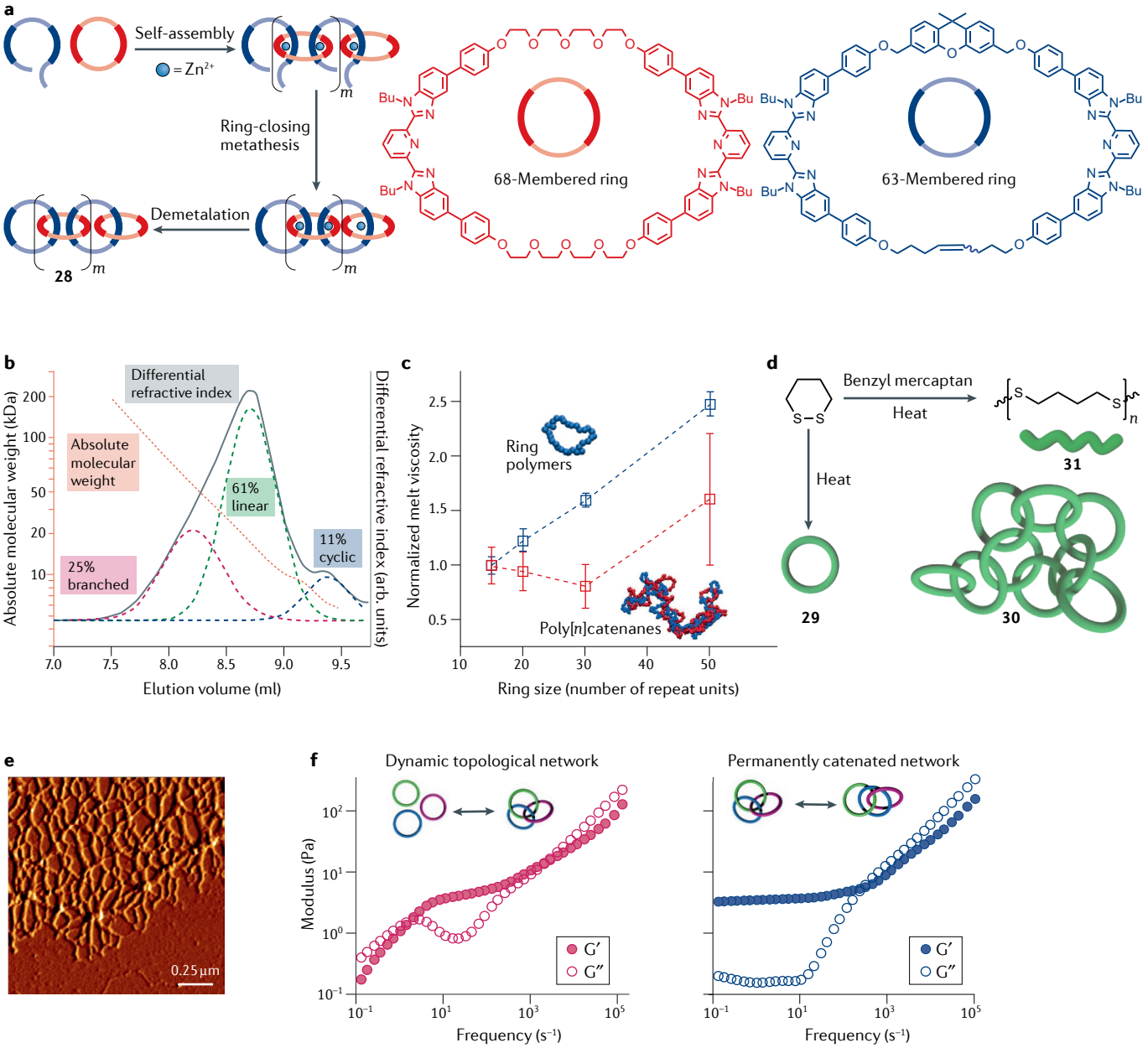

Fig. 9 | **Poly[*n*]catenanes and Olympic gels. a** | Synthetic steps used to access a poly[*n*]catenane (**28**) and the chemical structures of its components. **b** | The gel permeation chromatography trace of **28** suggests three unique architectures, identified as branched, linear and cyclic. **c** | Viscosity of ring polymer (blue) and poly[*n*]catenane (red) melts as a function of ring size as measured by molecular dynamics simulations. Data are normalized by the values at ring size = 15 repeat units. **d** | Polymerization of 1,2-dithiane, yielding cyclic polymer (**29**), catenated network (**30**) and linear polymer (**31**). **e** | An atomic force microscopy image of interlocked kinetoplast DNA. **f** | Dynamic light-scattering microrheology of Olympic gel, prepared using circular DNA and topoisomerase, shows multiple dynamical regimes (G′, shear storage modulus; G″, shear loss modulus). Panels **a** and **b** reprinted with permission from REF.[219], AAAS. Panel **c** (images) reprinted with permission from REF.[228], ACS. Panel **c** (graph) adapted with permission from REF.[229], AIP. Panel **e** reprinted with permission from REF.[243], Elsevier B.V. Panel **f** reprinted with permission from REF.[247], APS.

in solution[220,221,226,227] or the melt[228,229]. In solution, poly[*n*]catenanes are qualitatively similar to linear polymers at long length scales[220,226], but, recently, Dehaghani et al.[227] found that the polymer dimensions do not scale with ring size, *m*, according to the typical good solvent exponent (≈0.588), but, instead, show a somewhat stronger dependence, $R_g \sim m^{0.65}$. Rauscher et al.[221] studied the dynamics of poly[*n*]catenanes in solution and found that ring motion was significantly retarded by the mechanical bonds, in terms of both centre-of-mass motion and internal ring relaxations, showing an order of magnitude slowdown relative to free rings. These phenomena are qualitatively similar to those found in entangled polymer melts, suggesting that the unusual dynamics in these MIPs originate from topological effects. However, in poly[*n*]catenanes, these effects are found at short timescales and length scales, while in conventional linear polymers, they occur at longer scales, suggesting that poly[*n*]catenane materials may have unique dynamical and rheological responses at short timescales

or length scales. Furthermore, the effects are magnified by decreasing the ring size, suggesting that ring size is a key design parameter for these polymers. Interestingly, increasing the ring stiffness only modestly affected the dynamics of the MIPs, which may explain some of the properties of the experimentally studied poly[*n*]catenanes: the high rigidity of the segments will result in very high T_gs and the catenation will frustrate packing, resulting in brittle solids. However, the molecule will still be flexible (small and fast) in solution compared with linear analogues.

More recently, a study of model poly[*n*]catenanes in the melt[228,229] has found that their conformations are highly complex. In particular, the polymers are globular at low *DP*, which inhibits interchain entanglement; it was estimated that chains of $n \approx 45$ rings are required for polymer chain entanglement, regardless of ring size. The dynamics of the polymers are even more interesting: multiple sub-diffusive regimes are observed in the monomer mean-squared displacement, even though there are no reptation-type dynamics, and the stress relaxation in the systems is extremely fast[229]. These results can be qualitatively explained in terms of a separation of ring-like and chain-like dynamics, but this cannot account for the non-monotonic dependence of the viscosity on the ring size: the viscosity actually decreases with increasing ring size (that is, increasing polymer molecular weight) up to the critical ring size, above which the viscosity begins to increase (FIG. 9c). This behaviour deviates strongly from that of ordinary ring polymer melts (FIG. 9c) and its cause is not yet known, but it is hypothesized that inter-ring stress (or correlations) is a key factor. Such stress would be large for small rings but become smaller (and relax faster) for larger ones, thus, leading to the unusual behaviour. These results make it clear that poly[*n*]catenanes are not merely chemical curiosities but exciting polymer architectures with unexpected dynamical properties.

Olympic gels and polycatenane networks

The polymer consisting entirely of interlocked rings can be taken a step further to polycatenane networks, also known as Olympic gels (FIG. 8a, bottom right)[230]. These networks were first considered theoretically[230], and are a synthetic challenge. Some statistical methods of synthesis have been proposed[231,232] and, although simulations have shown that these methods can lead to network formation[233], such approaches have shown limited success in practice. Therefore, the material properties of Olympic gels have been studied primarily by theory[234] and simulation[235,236]. Several authors[237,238] have argued that the Young's modulus of a catenated network should be related to the average number of catenations (or mechanical bonds) per ring. If a ring is catenated by N_c of its neighbours, then it is divided into N_c elastically active strands, so that the modulus is given by $G = N_c p k_B T N^{-1}$ where p is the Kuhn segment density and N the number of Kuhn segments per ring. While this argument and other similar considerations have been used to estimate the number of catenations per ring in experimentally realized catenated networks (see below)[237,238], it is not clear under what circumstances the relation is valid. Indeed, when the elasticity of Olympic gels was examined theoretically via scaling arguments, it was found that the stress at small deformations was constant (zero modulus), but large deformations resulted in non-Hookean elasticity, with the force, f, being related to the deformation, λ, as $f \sim \lambda^{2/5}$, in contrast to classical rubbers, where the relationship is linear[234]. Such results suggest that Olympic gels will be considerably softer than conventional polymer networks.

In simulations, Olympic gels show a smaller degree of swelling for larger ring sizes[235,236], a result that is in strong contrast to chemically crosslinked gels, which show greater swelling when prepared from chains of larger molecular weight (or lower degree of crosslinking). This unusual behaviour has a complex topological origin. In particular, ring polymers may be highly entangled without being catenated, and these 'non-trapped' entanglements are released when the network swells with solvent, allowing further expansion than if the rings were catenated. However, the probability of finding two nearby non-catenated rings vanishes as the ring size increases — a famous result in knot theory — so that there are fewer non-trapped entanglements and, therefore, reduced swelling. How these non-trapped entanglements affect material properties such as elasticity and rheology has not yet been examined. Although simulations offer promising avenues for future research, it is important to pay close attention to how the systems are prepared because the method of gel preparation will undoubtedly alter the statistical and topological properties of the network.

One of the few reported synthetic approaches to what has been hypothesized as Olympic-like networks is the thermal polymerization of 1,2-dithiane. This method of polydisulfide synthesis was intended to target cyclic polymers[239]. However, the unique properties of the materials suggested the presence of catenated structures[237]. A thermally polymerized sample of polydithiane was fractionated via high-performance liquid chromatography, yielding two apparently different architectures: a small-molecular-weight cyclic polymer (**29**) and a potentially interlocked larger-molecular-weight polydithiane network (**30**). Interestingly, the viscoelastic properties of the proposed **30** fractions did not match those of linear analogues (**31**, prepared by polymerization of 1,2-dithiane in the presence of a small amount of benzyl mercaptan, FIG. 9d). For instance, the storage modulus of the interlocked **30** remained constant above the melting temperature (from 40 °C to 100 °C), forming a rubbery plateau, while the linear sample (**31**) flowed at these temperatures. Stress–strain experiments revealed that **30** was extremely flexible and could be stretched to 3,000% elongation without breaking under load and underwent instant recovery, but **31** broke at 800% strain. Since this initial report, materials with similar properties have been synthesized via thermal initiation of cyclic disulfides to make interlocked polymers with aromatic side groups[237] and an interlocked copolymer of dithiane and lipoic acid[240]. In these studies, rheological measurements were used as evidence of catenation, even though the relationship between the two is essentially unknown, apart from theoretical considerations that have not yet been

tested by simulation. Although the materials are likely catenated, there is no direct evidence supporting this conclusion, so these studies beg the question of how catenation affects rheological behaviour, providing impetus for future studies.

Although the confirmed synthesis of defined Olympic networks has been difficult to achieve in the lab, naturally occurring topological networks have been observed in the kinetoplast DNA[241–243]. Indeed, vast interlocked networks of several thousand circular DNA molecules have been observed by electron microscopy[244] (FIG. 9e). These interlocked network assemblies bypass the traditional synthetic obstacles and have inspired efforts to synthesize catenated materials from DNA[245,246]. For this methodology, topoisomerase enzymes are employed, which break and reform DNA chains, thereby, allowing them to 'pass through' one another. First, the enzymes are introduced to a concentrated solution of DNA rings, so that the rings regularly cross each other, resulting in a dynamic interlocked Olympic gel with transient catenations between the rings. Then, if the enzymes are inhibited in these dynamic DNA gels, the catenated network becomes permanent, as the chains can no longer break and reform[238,247]. The linear rheology for both the dynamic (active) and permanent (inactive) gels (FIG. 9f) demonstrates that, at timescales shorter than the activity of the topoisomerase, both materials experienced an elastic plateau associated with the interlocked network. However, at the longest timescales, the active (dynamic) gel relaxes all stresses (akin to a polymer solution), while the inactive gel remains solid-like. As a result, by inhibiting or stimulating topoisomerase activity, these materials can switch between the solid-like and fluid-like states. Despite these interesting results, several questions remain unanswered. For instance, the stress–strain behaviour of these gels has not been reported, and it is unclear how the conditions of gel preparation (for example, ring size and DNA volume fraction) affect the resulting material properties. Nevertheless, DNA-based Olympic gels have great potential because they are a facile route to interlocked catenane networks.

Outlook

While MIPs may have initially been targeted as an intriguing synthetic challenge or for their aesthetic appeal, studies have shown that these polymers offer unique property profiles that potentially provide advantages in a number of applications. Their utility is, perhaps, most clearly demonstrated through polyrotaxane-based materials such as SRMs; the facile scalable, and inexpensive synthesis of **1**, for example, has propelled the research beyond chemistry and into materials engineering. Over the past two decades, researchers have established relationships between structure and mechanical properties for such materials (at least at a qualitative level), while continued advances in material preparation and molecular simulations promise to further improve our understanding. As a result, these materials have already been applied towards (and, in some cases, even commercialized in) several technologies, such as Li-ion batteries and anti-scratch coatings. Most current applications of MIP-based materials rely on their excellent mechanical properties, but there are other ways to exploit the interlocked nature of these polymers, which have not yet been fully explored. For instance, polyrotaxanes have been successfully used as drug delivery vehicles and molecular wires, and the ability to incorporate controllable molecular machinery in polymer architectures may open the door to transducing molecular-scale work to the macroscale. Furthermore, recent research has suggested that the mechanical bond can improve ion mobility in solid polymer electrolytes[248]. In general, transport processes in MIPs are not well studied and represent an exciting opportunity for future research. Improving our understanding of such processes may allow MIPs to be incorporated into membranes or selective barrier coatings.

Despite the exciting opportunities described above, the field is also plagued by certain challenges, and chief among these are the difficulties of chemical synthesis. New synthetic strategies are required to expand the library of interlocked architectures and synthesize these new MIPs in quantities large enough for detailed material characterization, both of which are major challenges, especially for the polycatenane materials. While CD-based MIPs have provided access to a wealth of exciting and useful materials, a greater diversity of MIP ring components would dramatically expand the materials design space. However, moving beyond CDs necessitates synthesizing rings, which is typically low yielding and may require arduous product isolation; the problem is magnified when targeting materials with many rings, such as poly[*n*]catenanes and Olympic gels. Progress in this field could be expedited with the development of high-yielding (bio)synthetic methodologies that allow access to rings other than CDs in large quantities. In light of these challenges, molecular simulations represent a powerful tool for developing fundamental physical understanding of MIPs. Indeed, these studies may be used to direct chemists towards high-value synthetic targets for specific applications. This kind of interdisciplinary approach has been applied successfully in many other areas of polymer science and represents an exciting future for MIPs.

1. Schill, G. & Zollenkopf, H. Rotaxan-verbindungen, 1. *Liebigs Ann.* **721**, 53–74 (1969).
2. Wasserman, E. The preparation of interlocking rings: a catenane. *J. Am. Chem. Soc.* **82**, 4433–4434 (1960).
3. Dietrich-Buchecker, C. O. & Sauvage, J.-P. A synthetic molecular trefoil knot. *Angew. Chem. Int. Ed.* **28**, 189–192 (1989).
4. Chichak, K. S. Molecular borromean rings. *Science* **304**, 1308–1312 (2004).
5. Richards, V. Molecular machines. *Nat. Chem.* **8**, 1090–1090 (2016).
6. Sauvage, J.-P. From chemical topology to molecular machines (Nobel Lecture). *Angew. Chem. Int. Ed.* **56**, 11080–11093 (2017).
7. Feringa, B. L. The art of building small: from molecular switches to motors (Nobel Lecture). *Angew. Chem. Int. Ed.* **56**, 11060–11078 (2017).
8. Stoddart, J. F. Mechanically interlocked molecules (MIMs)—molecular shuttles, switches, and machines (Nobel Lecture). *Angew. Chem. Int. Ed.* **56**, 11094–11125 (2017).
9. Cotí, K. K. et al. Mechanised nanoparticles for drug delivery. *Nanoscale* **1**, 16–39 (2009).
10. Garcia-Rio, L., Otero-Espinar, F. J., Luzardo-Alvarez, A. & Blanco-Mendez, J. Cyclodextrin based rotaxanes, polyrotaxanes and polypseudorotaxanes and their biomedical applications. *Curr. Top. Med. Chem.* **14**, 478–493 (2014).
11. Zhang, Y. M., Liu, Y. H. & Liu, Y. Cyclodextrin-based multistimuli-responsive supramolecular assemblies and their biological functions. *Adv. Mater.* **32**, 1806158 (2019).

12. Zhang, J. & Ma, P. X. Cyclodextrin-based supramolecular systems for drug delivery: Recent progress and future perspective. *Adv. Drug Deliv. Rev.* **65**, 1215–1233 (2013).
13. Neal, E. A. & Goldup, S. M. Chemical consequences of mechanical bonding in catenanes and rotaxanes: isomerism, modification, catalysis and molecular machines for synthesis. *Chem. Commun.* **50**, 5128–5142 (2014).
14. Evans, N. H. & Beer, P. D. Progress in the synthesis and exploitation of catenanes since the Millennium. *Chem. Soc. Rev.* **43**, 4658–4683 (2014).
15. Leigh, D. A., Marcos, V. & Wilson, M. R. Rotaxane catalysts. *ACS Catal.* **4**, 4490–4497 (2014).
16. Beves, J. E., Blight, B. A., Campbell, C. J., Leigh, D. A. & McBurney, R. T. Strategies and tactics for the metal-directed synthesis of rotaxanes, knots, catenanes, and higher order links. *Angew. Chem. Int. Ed.* **50**, 9260–9327 (2011).
17. Hubin, T. J. & Busch, D. H. Template routes to interlocked molecular structures and orderly molecular entanglements. *Coord. Chem. Rev.* **200–202**, 5–52 (2000).
18. Niu, Z. & Gibson, H. W. Polycatenanes. *Chem. Rev.* **109**, 6024–6046 (2009).
19. Fang, L. et al. Mechanically bonded macromolecules. *Chem. Soc. Rev.* **39**, 17–29 (2010).
20. Arunachalam, M. & Gibson, H. W. Recent developments in polypseudorotaxanes and polyrotaxanes. *Prog. Polym. Sci.* **39**, 1043–1073 (2014).
21. Takata, T., Kihara, N. & Furusho, Y. Polyrotaxanes and polycatenanes: recent advances in syntheses and applications of polymers comprising of interlocked structures. *Adv. Polym. Sci.* **171**, 1–75 (2004).
22. Huang, F. H. & Gibson, H. W. Polypseudorotaxanes and polyrotaxanes. *Prog. Polym. Sci.* **30**, 982–1018 (2005).
23. Harrison, I. T. & Harrison, S. Synthesis of a stable complex of a macrocycle and a threaded chain. *J. Am. Chem. Soc.* **89**, 5723–5724 (1967).
24. Wenz, G. & Keller, B. Threading cyclodextrin rings on polymer chains. *Angew. Chem. Int. Ed. Engl.* **31**, 197–199 (1992).
25. Harada, A. The molecular necklace: a rotaxane containing many threaded α-cyclodextrins. *Nature* **356**, 325–327 (1992).
26. Fleury, G. et al. Synthesis and characterization of high molecular weight polyrotaxanes: Towards the control over a wide range of threaded α-cyclodextrins. *Soft Matter* **1**, 378–385 (2005).
27. Miyake, K. et al. Formation process of cyclodextrin necklace–analysis of hydrogen bonding on a molecular level. *J. Am. Chem. Soc.* **125**, 5080–5085 (2003).
28. Inomata, A. et al. Crystallinity and cooperative motions of cyclic molecules in partially threaded solid-state polyrotaxanes. *Macromolecules* **43**, 4660–4666 (2010).
29. Kato, K., Mizusawa, T., Yokoyama, H. & Ito, K. Polyrotaxane glass: peculiar mechanics attributable to the isolated dynamics of different components. *J. Phys. Chem. Lett.* **6**, 4043–4048 (2015).
30. Mayumi, K. & Ito, K. Structure and dynamics of polyrotaxane and slide-ring materials. *Polymer* **51**, 959–967 (2010).
31. Zhao, C. et al. Sliding mode of cyclodextrin in polyrotaxane and slide-ring gel. *J. Phys. Condens. Matter* **17**, S2841–S2846 (2005).
32. Yasuda, Y. et al. Molecular dynamics of polyrotaxane in solution investigated by quasi-elastic neutron scattering and molecular dynamics simulation: sliding motion of rings on polymer. *J. Am. Chem. Soc.* **141**, 9655–9663 (2019).
33. Yasuda, Y. et al. Sliding dynamics of ring on polymer in rotaxane: a coarse-grained molecular dynamics simulation study. *Macromolecules* **52**, 3787–3793 (2019).
34. Mayumi, K. et al. Concentration-induced conformational change in linear polymer threaded into cyclic molecules. *Macromolecules* **41**, 6480–6485 (2008).
35. Yamada, S., Sanada, Y., Tamura, A., Yui, N. & Sakurai, K. Chain architecture and flexibility of α-cyclodextrin/PEG polyrotaxanes in dilute solutions. *Polym. J.* **47**, 464–467 (2015).
36. Gibson, H. W., Liu, S., Gong, C., Ji, Q. & Joseph, E. Studies of the formation of poly(ester rotaxane)s from diacid chlorides, diols, and crown ethers and their properties. *Macromolecules* **30**, 3711–3727 (1997).
37. Gong, C. & Gibson, H. W. Controlling microstructure in polymeric molecular shuttles: Solvent-induced localization of macrocycles in poly(urethane/crown ether) rotaxanes. *Angew. Chem. Int. Ed. Engl.* **36**, 2331–2333 (1997).
38. Shen, Y. X., Xie, D. & Gibson, H. W. Polyrotaxanes Based on polyurethane backbones and crown ether cyclics. 1. Synthesis. *J. Am. Chem. Soc.* **116**, 537–548 (1994).
39. Gong, C., Glass, T. E. & Gibson, H. W. Poly(urethane/crown ether rotaxane)s with solvent switchable microstructures. *Macromolecules* **31**, 308–313 (1998).
40. Gong, C., Ji, Q., Subramaniam, C. & Gibson, H. W. Main chain polyrotaxanes by threading crown ethers onto a preformed polyurethane: preparation and properties. *Macromolecules* **31**, 1814–1818 (1998).
41. Gong, C. & Gibson, H. W. Synthesis and characterization of a polyester/crown ether rotaxane derived from a difunctional blocking group. *Macromolecules* **29**, 7029–7033 (1996).
42. Gong, C. G. & Gibson, H. W. Polyrotaxanes and related structures: Synthesis and properties. *Curr. Opin. Solid State Mater. Sci.* **2**, 647–652 (1997).
43. Gong, C. & Gibson, H. W. Dethreading during the preparation of polyrotaxanes. *Macromol. Chem. Phys.* **198**, 2321–2332 (1997).
44. Chen, Z. et al. Effect of component mobility on the properties of macromolecular [2]rotaxanes. *Angew. Chem. Int. Ed.* **55**, 2778–2781 (2016).
45. Uenuma, S. et al. Drastic change of mechanical properties of polyrotaxane bulk: ABA–BAB sequence change depending on ring position. *ACS Macro Lett.* **8**, 140–144 (2019).
46. Uenuma, S. et al. Self-assembled structure of polyrotaxane consisting of β-cyclodextrin and poly(ethylene oxide)-*block*-poly(propylene oxide)-*block*-poly(ethylene oxide) triblock copolymer in bulk system. *Chem. Lett.* **45**, 991–993 (2016).
47. Lin, Q., Li, L., Tang, M., Hou, X. & Ke, C. Rapid macroscale shape morphing of 3D-printed polyrotaxane monoliths amplified from pH-controlled nanoscale ring motions. *J. Mater. Chem. C* **6**, 11956–11960 (2018).
48. Lin, Q., Hou, X. & Ke, C. Ring shuttling controls macroscopic motion in a three-dimensional printed polyrotaxane monolith. *Angew. Chem. Int. Ed. Engl.* **56**, 4452–4457 (2017).
49. Lin, Q., Tang, M. & Ke, C. Thermo-responsive 3D-printed polyrotaxane monolith. *Polym. Chem.* **11**, 304–308 (2020).
50. Kato, K., Nemoto, K., Mayumi, K., Yokoyama, H. & Ito, K. Ductile glass of polyrotaxane toughened by stretch-induced intramolecular phase separation. *ACS Appl. Mater. Interfaces* **9**, 32436–32440 (2017).
51. Kato, K., Mizusawa, T., Yokoyama, H. & Ito, K. Effect of topological constraint and confined motions on the viscoelasticity of polyrotaxane glass with different interactions between rings. *J. Phys. Chem. C* **121**, 1861–1869 (2017).
52. Kato, K., Ohara, A., Yokoyama, H. & Ito, K. Prolonged glass transition due to topological constraints in polyrotaxanes. *J. Am. Chem. Soc.* **141**, 12502–12506 (2019).
53. Cardin, D. J. Encapsulated conducting polymers. *Adv. Mater.* **14**, 553–563 (2002).
54. Mayumi, K., Ito, K. & Kato, K. *Polyrotaxane and Slide-Ring Materials* (Royal Society of Chemistry, 2015).
55. Frampton, M. J. & Anderson, H. L. Insulated molecular wires. *Angew. Chem. Int. Ed. Engl.* **46**, 1028–1064 (2007).
56. Terao, J., Tang, A., Michels, J. J., Krivokapic, A. & Anderson, H. L. Synthesis of poly(*para*-phenylenevinylene) rotaxanes by aqueous Suzuki coupling. *Chem. Commun*. 56–57 (2004).
57. Cacialli, F. et al. Cyclodextrin-threaded conjugated polyrotaxanes as insulated molecular wires with reduced interstrand interactions. *Nat. Mater.* **1**, 160–164 (2002).
58. Taylor, P. N. et al. Insulated molecular wires: synthesis of conjugated polyrotaxanes by Suzuki coupling in water. *Angew. Chem. Int. Ed. Engl.* **39**, 3456–3460 (2000).
59. Michels, J. J. et al. Synthesis of conjugated polyrotaxanes. *Chem. Eur. J.* **9**, 6167–6176 (2003).
60. van den Boogaard, M. et al. Synthesis of insulated single-chain semiconducting polymers based on polythiophene, polyfluorene, and β-cyclodextrin. *Chem. Mater.* **16**, 4383–4385 (2004).
61. Ikeda, T., Higuchi, M. & Kurth, D. G. From thiophene [2]rotaxane to polythiophene polyrotaxane. *J. Am. Chem. Soc.* **131**, 9158–9159 (2009).
62. Farcas, A. et al. Molecular wire formation from poly[2,7-(9,9-dioctylfluorene)-alt-(5,5′-bithiophene/cucurbit[7]uril)] polyrotaxane copolymer. *Eur. Polym. J.* **62**, 124–129.
63. Belosludov, R. V., Mizuseki, H., Ichinoseki, K. & Kawazoe, Y. Theoretical study on inclusion complex of polyaniline covered by cyclodextrins for molecular device. *Jpn. J. Appl. Phys.* **41**, 2739–2741 (2002).
64. Belosludov, R. V. et al. Molecular enamel wires for electronic devices: Theoretical study. *Jpn. J. Appl. Phys.* **42**, 2492–2494 (2003).
65. Brovelli, S. et al. Tuning intrachain versus interchain photophysics via control of the threading ratio of conjugated polyrotaxanes. *Nano Lett.* **8**, 4546–4551 (2008).
66. Oddy, F. E. et al. Influence of cyclodextrin size on fluorescence quenching in conjugated polyrotaxanes by methyl viologen in aqueous solution. *J. Mater. Chem.* **19**, 2846–2852 (2009).
67. Farcas, A. et al. Cucurbit[7]uril-threaded poly(3,4-ethylenedioxythiophene): a novel processable conjugated polyrotaxane. *Eur. J. Org. Chem.* **2019**, 3442–3450 (2019).
68. Terao, J. & Tsuji, Y. New synthetic methods of π-conjugated inclusion complexes with high conductivity. *J. Incl. Phenom. Macrocycl. Chem.* **80**, 165–175 (2014).
69. Grigoras, M. & Stafie, L. Electrically insulated molecular wires. *Supramol. Chem.* **22**, 237–248 (2010).
70. Terao, J. et al. Insulated molecular wire with highly conductive π-conjugated polymer core. *J. Am. Chem. Soc.* **131**, 18046–18047 (2009).
71. Terao, J. et al. Design principle for increasing charge mobility of π-conjugated polymers using regularly localized molecular orbitals. *Nat. Commun.* **4**, 1691 (2013).
72. Wankar, J. et al. Recent advances in host–guest self-assembled cyclodextrin carriers: implications for responsive drug delivery and biomedical engineering. *Adv. Funct. Mater.* **30**, 1909049 (2020).
73. Tamura, A. & Yui, N. Threaded macromolecules as a versatile framework for biomaterials. *Chem. Commun.* **50**, 13433–13446 (2014).
74. Li, J. J., Zhao, F. & Li, J. Polyrotaxanes for applications in life science and biotechnology. *Appl. Microbiol. Biotechnol.* **90**, 427–443 (2011).
75. Loethen, S., Kim, J.-M. & Thompson, D. H. Biomedical applications of cyclodextrin based polyrotaxanes. *Polym. Rev.* **47**, 383–418 (2007).
76. Arisaka, Y. & Yui, N. Polyrotaxane-based biointerfaces with dynamic biomaterial functions. *J. Mater. Chem. B* **7**, 2123–2129 (2019).
77. Yui, N. & Ooya, T. Molecular mobility of interlocked structures exploiting new functions of advanced biomaterials. *Chem. Eur. J.* **12**, 6730–6737 (2006).
78. Patel, P., Pol, A., Jain, R. & Dandekar, P. in *Encyclopedia of Biomedical Polymers and Polymeric Biomaterials* (ed. Mishra, M.) (CRC Press, 2015).
79. Ooya, T. et al. Effects of polyrotaxane structure on polyion complexation with DNA. *Sci. Technol. Adv. Mater.* **5**, 363–369 (2004).
80. Ooya, T. et al. Biocleavable polyrotaxane-plasmid DNA polyplex for enhanced gene delivery. *J. Am. Chem. Soc.* **128**, 3852–3853 (2006).
81. Mammen, M., Choi, S.-K. & Whitesides, G. M. Polyvalent interactions in biological systems: implications for design and use of mMultivalent ligands and inhibitors. *Angew. Chem. Int. Ed. Engl.* **37**, 2754–2794 (1998).
82. Seo, J.-H. et al. Inducing rapid cellular response on RGD-binding threaded macromolecular surfaces. *J. Am. Chem. Soc.* **135**, 5513–5516 (2013).
83. Ooya, T., Eguchi, M. & Yui, N. Supramolecular design for multivalent interaction: maltose mobility along polyrotaxane enhanced binding with concanavalin A. *J. Am. Chem. Soc.* **125**, 13016–13017 (2003).
84. Sluysmans, D. & Stoddart, J. F. The burgeoning of mechanically interlocked molecules in chemistry. *Trends Chem.* **1**, 185–197 (2019).
85. Berná, J. et al. Macroscopic transport by synthetic molecular machines. *Nat. Mater.* **4**, 704–710 (2005).
86. Sun, X. et al. Towards the self-assembly of polyrotaxanes. *Macromol. Symp.* **77**, 191–207 (1994).
87. Zhang, W. et al. Folding of a donor–acceptor polyrotaxane by using noncovalent bonding interactions. *Proc. Natl Acad. Sci. USA* **105**, 6514–6519 (2008).
88. Zhu, Z. et al. Synthesis and solution-state dynamics of donor–acceptor oligorotaxane foldamers. *Chem. Sci.* **4**, 1470–1483 (2013).
89. Basu, S. et al. Donor–acceptor oligorotaxanes made to order. *Chem. Eur. J.* **17**, 2107–2119 (2011).
90. Zhu, Z. et al. Oligomeric pseudorotaxanes adopting infinite-chain lattice superstructures. *Angew. Chem. Int. Ed. Engl.* **51**, 7231–7235 (2012).
91. Sluysmans, D. et al. Synthetic oligorotaxanes exert high forces when folding under mechanical load. *Nat. Nanotechnol.* **13**, 209–213 (2018).
92. Sluysmans, D., Devaux, F., Bruns, C. J., Stoddart, J. F. & Duwez, A.-S. Dynamic force spectroscopy of synthetic

oligorotaxane foldamers. *Proc. Natl Acad. Sci. USA* **115**, 9362–9366 (2018).
93. Pezzato, C. et al. An efficient artificial molecular pump. *Tetrahedron* **73**, 4849–4857 (2017).
94. Qiu, Y. et al. A molecular dual pump. *J. Am. Chem. Soc.* **141**, 17472–17476 (2019).
95. Qiu, Y. et al. A precise polyrotaxane synthesizer. *Science* **368**, 1247–1253 (2020).
96. Whittaker, A. K. in *Modern Magnetic Resonance* (ed. Webb, G. A.) 583–589 (Springer, 2006).
97. Okumura, Y. & Ito, K. The polyrotaxane gel: a topological gel by figure-of-eight cross-links. *Adv. Mater.* **13**, 485–487 (2001).
98. Ito, K. Slide-ring materials using topological supramolecular architecture. *Curr. Opin. Solid State Mater. Sci.* **14**, 28–34 (2010).
99. Karino, T., Okumura, Y., Ito, K. & Shibayama, M. SANS studies on spatial inhomogeneities of slide-ring gels. *Macromolecules* **37**, 6177–6182 (2004).
100. Liu, C., Kadono, H., Yokoyama, H., Mayumi, K. & Ito, K. Crack propagation resistance of slide-ring gels. *Polymer* **181**, 121782 (2019).
101. Kato, K., Ikeda, Y. & Ito, K. Direct determination of cross-link density and its correlation with the elastic modulus of a gel with slidable cross-links. *ACS Macro Lett.* **8**, 700–704 (2019).
102. Jiang, L. et al. Highly stretchable and instantly recoverable slide-ring gels consisting of enzymatically synthesized polyrotaxane with low host coverage. *Chem. Mater.* **30**, 5013–5019 (2018).
103. Wang, Z. et al. Highly stretchable and compressible shape memory hydrogels based on polyurethane network and supramolecular interaction. *Mater. Today Commun.* **17**, 246–251 (2018).
104. Kato, K., Karube, K., Nakamura, N. & Ito, K. The effect of ring size on the mechanical relaxation dynamics of polyrotaxane gels. *Polym. Chem.* **6**, 2241–2248 (2015).
105. Liu, C. et al. Direct observation of large deformation and fracture behavior at the crack tip of slide-ring gel. *J. Electrochem. Soc.* **166**, B3143–B3147 (2019).
106. Higgs, P. G. & Ball, R. C. Trapped entanglements in rubbers. A unification of models. *Europhys. Lett.* **8**, 357–361 (1989).
107. Kość, M. "Belt-loop" model of chain entanglement. *Colloid Polym. Sci.* **266**, 105–113 (1988).
108. Adolf, D. Origins of entanglement effects in rubber elasticity. *Macromolecules* **21**, 228–230 (1988).
109. Kholodenko, A. L. & Vilgis, T. A. Some geometrical and topological problems in polymer physics. *Phys. Rep.* **298**, 251–370 (1998).
110. Edwards, S. F. & Vilgis, T. The effect of entanglements in rubber elasticity. *Polymer* **27**, 483–492 (1986).
111. Graessley, W. W. & Pearson, D. S. Stress–strain behavior in polymer networks containing nonlocalized junctions. *J. Chem. Phys.* **66**, 3363–3370 (1977).
112. Ziabicki, A. Contribution of entrapped entanglements to equilibrium elasticity of rubber networks. *Colloid Polym. Sci.* **254**, 1–5 (1976).
113. Marrucci, G. A mechanical model for rubbers containing entanglements. *Rheol. Acta* **18**, 193–198 (1979).
114. Ito, K. Novel cross-linking concept of polymer network: synthesis, structure, and properties of slide-ring gels with freely movable junctions. *Polym. J.* **39**, 489–499 (2007).
115. Yasuda, Y. et al. Molecular dynamics simulation and theoretical model of elasticity in slide-ring gels. *ACS Macro Lett.* **9**, 1280–1285 (2020).
116. Kato, K., Yasuda, T. & Ito, K. Viscoelastic properties of slide-ring gels reflecting sliding dynamics of partial chains and entropy of ring components. *Macromolecules* **46**, 310–316 (2013).
117. Fleury, G., Schlatter, G., Brochon, C. & Hadziioannou, G. From high molecular weight precursor polyrotaxanes to supramolecular sliding networks. The 'sliding gels'. *Polymer* **46**, 8494–8501 (2005).
118. Rubinstein, M. & Colby, R. H. *Polymer Physics* (Oxford Univ. Press, 2003).
119. Koga, T. & Tanaka, F. Elastic properties of polymer networks with sliding junctions. *Eur. Phys. J. E* **17**, 225–229 (2005).
120. Zhang, Z. et al. Designing the slide-ring polymer network with both good mechanical and damping properties via molecular dynamics simulation. *Polymers* **10**, 964 (2018).
121. Gavrilov, A. A. & Potemkin, I. I. Adaptive structure of gels and microgels with sliding cross-links: enhanced softness, stretchability and permeability. *Soft Matter* **14**, 5098–5105 (2018).
122. Karino, T. et al. SANS studies on deformation mechanism of slide-ring gel. *Macromolecules* **38**, 6161–6167 (2005).
123. Karino, T., Shibayama, M., Okumura, Y. & Ito, K. SANS study on pulley effect of slide-ring gel. *Phys. B Condens. Matter* **385–386**, 807–809 (2006).
124. Shinohara, Y. et al. Small-angle X-ray scattering study of the pulley effect of slide-ring gels. *Macromolecules* **39**, 7386–7391 (2006).
125. Kato, K., Yasuda, T. & Ito, K. Peculiar elasticity and strain hardening attributable to counteracting entropy of chain and ring in slide-ring gels. *Polymer* **55**, 2614–2619 (2014).
126. Mayumi, K., Tezuka, M., Bando, A. & Ito, K. Mechanics of slide-ring gels: novel entropic elasticity of a topological network formed by ring and string. *Soft Matter* **8**, 8179–8183 (2012).
127. de Gennes, P.-G. Sliding gels. *Phys. A* **271**, 231–237 (1999).
128. Tonks, L. The complete equation of state of one, two and three-dimensional gases of hard elastic spheres. *Phys. Rev.* **50**, 955–963 (1936).
129. Sevick, E. M. & Williams, D. R. M. Piston-rotaxanes as molecular shock absorbers. *Langmuir* **26**, 5864–5868 (2010).
130. Gao, Y., Williams, D. R. M. & Sevick, E. M. Dynamics of molecular shock-absorbers: Energy dissipation and the fluctuation theorem. *Soft Matter* **7**, 5739–5744 (2011).
131. Pinson, M. B., Sevick, E. M. & Williams, D. R. M. Mobile rings on a polyrotaxane lead to a yield force. *Macromolecules* **46**, 4191–4197 (2013).
132. Boesten, R. J. J., Sevick, E. M. & Williams, D. R. M. Piston rotaxane monolayers: shear swelling and nanovalve behavior. *Macromolecules* **43**, 7244–7249 (2010).
133. Sevick, E., Williams, D., Sevick, E. M. & Williams, D. R. M. A piston-rotaxane with two potential stripes: force transitions and yield stresses. *Molecules* **18**, 13398–13409 (2013).
134. Metzler, R., Kantor, Y. & Kardar, M. Force-extension relations for polymers with sliding links. *Phys. Rev. E* **66**, 022102 (2002).
135. Ito, K. Novel entropic elasticity of polymeric materials: why is slide-ring gel so soft? *Polym. J.* **44**, 38–41 (2012).
136. Müller, T., Sommer, J.-U. & Lang, M. Tendomers – force sensitive bis-rotaxanes with jump-like deformation behavior. *Soft Matter* **15**, 3671–3679 (2019).
137. Kato, K., Okabe, Y., Okazumi, Y. & Ito, K. A significant impact of host–guest stoichiometry on the extensibility of polyrotaxane gels. *Chem. Commun.* **51**, 16180–16183 (2015).
138. Murakami, T., Schmidt, B. V. K. J., Brown, H. R. & Hawker, C. J. Structural versatility in slide-ring gels: influence of co-threaded cyclodextrin spacers. *J. Polym. Sci. A Polym. Chem.* **55**, 1156–1165 (2017).
139. Liu, C., Kadono, H., Yokoyama, H., Mayumi, K. & Ito, K. Crack propagation resistance of slide-ring gels. *Polymer* **181**, 121782 (2019).
140. Araki, J., Kataoka, T. & Ito, K. Preparation of a "sliding graft copolymer", an organic solvent-soluble polyrotaxane containing mobile side chains, and its application for a crosslinked elastomeric supramolecular film. *Soft Matter* **4**, 245–249 (2008).
141. Kato, K., Hori, A. & Ito, K. An efficient synthesis of low-covered polyrotaxanes grafted with poly(ε-caprolactone) and the mechanical properties of its cross-linked elastomers. *Polymer* **147**, 67–73 (2018).
142. Li, X. et al. Highly toughened polylactide with novel sliding graft copolymer by in situ reactive compatibilization, crosslinking and chain extension. *Polymer* **55**, 4313–4323 (2014).
143. Fleury, G., Schlatter, G., Brochon, C. & Hadziioannou, G. Unveiling the sliding motion in topological networks: influence of the swelling solvent on the relaxation dynamics. *Adv. Mater.* **18**, 2847–2851 (2006).
144. Fleury, G. et al. Topological polymer networks with sliding cross-link points: The "sliding gels". Relationship between their molecular structure and the viscoelastic as well as the swelling properties. *Macromolecules* **40**, 535–543 (2007).
145. Sawada, J., Aoki, D., Otsuka, H. & Takata, T. A guiding principle for strengthening crosslinked polymers: synthesis and application of mobility-controlling rotaxane crosslinkers. *Angew. Chem. Int. Ed. Engl.* **58**, 2765–2768 (2019).
146. Koyama, Y. Synthesis of topologically crosslinked polymers with rotaxane-crosslinking points. *Polym. J.* **46**, 315–322 (2014).
147. Sawada, J., Aoki, D., Uchida, S., Otsuka, H. & Takata, T. Synthesis of vinylic macromolecular rotaxane cross-linkers endowing network polymers with toughness. *ACS Macro Lett.* **4**, 598–601 (2015).
148. Iijima, K., Aoki, D., Otsuka, H. & Takata, T. Synthesis of rotaxane cross-linked polymers with supramolecular cross-linkers based on γ-CD and PTHF macromonomers: The effect of the macromonomer structure on the polymer properties. *Polymer* **128**, 392–396 (2017).
149. Tan, S., Blencowe, A., Ladewig, K. & Qiao, G. G. A novel one-pot approach towards dynamically cross-linked hydrogels. *Soft Matter* **9**, 5239–5250 (2013).
150. Sawada, J., Aoki, D., Sun, Y., Nakajima, K. & Takata, T. Effect of coexisting covalent cross-links on the properties of rotaxane-cross-linked polymers. *ACS Appl. Polym. Mater.* **2**, 1061–1064 (2020).
151. Noda, Y., Hayashi, Y. & Ito, K. From topological gels to slide-ring materials. *J. Appl. Polym. Sci.* **131**, 40509 (2014).
152. Minato, K. et al. Mechanical properties of supramolecular elastomers prepared from polymer-grafted polyrotaxane. *Polymer* **128**, 386–391 (2017).
153. Koyanagi, K., Takashima, Y., Yamaguchi, H. & Harada, A. Movable cross-linked polymeric materials from bulk polymerization of reactive polyrotaxane cross-linker with acrylate monomers. *Macromolecules* **50**, 5695–5700 (2017).
154. Shi, C.-Y. et al. An ultrastrong and highly stretchable polyurethane elastomer enabled by a zipper-like ring-sliding effect. *Adv. Mater.* **32**, 2000345 (2020).
155. Oku, T., Furusho, Y. & Takata, T. A concept for recyclable cross-linked polymers: Topologically networked polyrotaxane capable of undergoing reversible assembly and disassembly. *Angew. Chem. Int. Ed. Engl.* **43**, 966–969 (2004).
156. Bilig, T. et al. Polyrotaxane networks formed via rotaxanation utilizing dynamic covalent chemistry of disulfide. *Macromolecules* **41**, 8496–8503 (2008).
157. Kohsaka, Y., Nakazono, K., Koyama, Y., Asai, S. & Takata, T. Size-complementary rotaxane cross-linking for the stabilization and degradation of a supramolecular network. *Angew. Chem. Int. Ed. Engl.* **50**, 4872–4875 (2011).
158. Sugihara, N. et al. Ion-conductive and elastic slide-ring gel Li electrolytes swollen with ionic liquid. *Electrochim. Acta* **229**, 166–172 (2017).
159. Zhuo, Y. et al. An ultra-durable icephobic coating by a molecular pulley. *Soft Matter* **15**, 3607–3611 (2019).
160. Choi, S., Kwon, T., Coskun, A. & Choi, J. W. Highly elastic binders integrating polyrotaxanes for silicon microparticle anodes in lithium ion batteries. *Science* **357**, 279–283 (2017).
161. Yoo, D.-J. et al. Highly elastic polyrotaxane binders for mechanically stable lithium hosts in lithium-metal batteries. *Adv. Mater.* **31**, 1901645 (2019).
162. Rowan, S. J., Cantrill, S. J., Cousins, G. R. L., Sanders, J. K. M. & Stoddart, J. F. Dynamic covalent chemistry. *Angew. Chem. Int. Ed. Engl.* **41**, 898–952 (2002).
163. Nakahata, M., Mori, S., Takashima, Y., Yamaguchi, H. & Harada, A. Self-healing materials formed by cross-linked polyrotaxanes with reversible bonds. *Chem* **1**, 766–775 (2016).
164. Zheng, S. Y. et al. Slide-ring cross-links mediated tough metallosupramolecular hydrogels with superior self-recoverability. *Macromolecules* **52**, 6748–6755 (2019).
165. Sood, N., Bhardwaj, A., Mehta, S. & Mehta, A. Stimuli-responsive hydrogels in drug delivery and tissue engineering. *Drug Deliv.* **23**, 748–770 (2016).
166. Imran, A. Bin, Seki, T. & Takeoka, Y. Recent advances in hydrogels in terms of fast stimuli responsiveness and superior mechanical performance. *Polym. J.* **42**, 839–851 (2010).
167. Koetting, M. C., Peters, J. T., Steichen, S. D. & Peppas, N. A. Stimulus-responsive hydrogels: Theory, modern advances, and applications. *Mater. Sci. Eng. R Rep.* **93**, 1–49 (2015).
168. Sakai, T. et al. Photoresponsive slide-ring gel. *Adv. Mater.* **19**, 2023–2025 (2007).
169. Haq, M. A., Su, Y. & Wang, D. Mechanical properties of PNIPAM based hydrogels: A review. *Mater. Sci. Eng. C* **70**, 842–855 (2017).
170. Imran, A. Bin, Seki, T., Ito, K. & Takeoka, Y. Poly(*N*-isopropylacrylamide) gel prepared using a hydrophilic polyrotaxane-based movable cross-linker. *Macromolecules* **43**, 1975–1980 (2010).
171. Bin Imran, A. et al. Extremely stretchable thermosensitive hydrogels by introducing slide-ring polyrotaxane cross-linkers and ionic groups into the polymer network. *Nat. Commun.* **5**, 5124 (2014).
172. Ohmori, K. et al. Molecular weight dependency of polyrotaxane-cross-linked polymer gel extensibility. *Chem. Commun.* **52**, 13757–13759 (2016).

173. Kobayashi, Y., Zheng, Y., Takashima, Y., Yamaguchi, H. & Harada, A. Physical and adhesion properties of supramolecular hydrogels cross-linked by movable cross-linking molecule and host-guest interactions. *Chem. Lett.* **47**, 1387–1390 (2018).
174. Ikura, R. et al. Preparation of hydrophilic polymeric materials with movable cross-linkers and their mechanical property. *Polymer* **196**, 122465 (2020).
175. Yasumoto, A. et al. Highly responsive hydrogel prepared using poly(*N*-isopropylacrylamide)-grafted polyrotaxane as a building block designed by reversible deactivation radical polymerization and click chemistry. *Macromolecules* **50**, 364–374 (2017).
176. Seo, J., Yui, N. & Seo, J.-H. Development of a supramolecular accelerator simultaneously to increase the cross-linking density and ductility of an epoxy resin. *Chem. Eng. J.* **356**, 303–311 (2019).
177. Wang, X.-S. et al. Relaxation and reinforcing effects of polyrotaxane in an epoxy resin matrix. *Macromolecules* **39**, 1046–1052 (2006).
178. Levita, G., Petris, De, Marchetti, S., Lazzeri, A. & Crosslink, A. Density and fracture toughness of epoxy resins. *J. Mater. Sci.* **26**, 2348–2352 (1991).
179. Ohtsuka, K. & Zhao, C. Properties of bismaleimide resin modified with polyrotaxane as a stress relaxation material. *Polym. Int.* **67**, 1112–1117 (2018).
180. Li, X. et al. Miscibility, intramolecular specific interactions and mechanical properties of a DGEBA based epoxy resin toughened with a sliding graft copolymer. *Chinese J. Polym. Sci.* **33**, 433–443 (2015).
181. Seo, J., Moon, S. W., Kang, H., Choi, B.-H. & Seo, J.-H. Foldable and extremely scratch-resistant hard coating materials from molecular necklace-like cross-linkers. *ACS Appl. Mater. Interfaces* **11**, 27306–27317 (2019).
182. Pruksawan, S., Samitsu, S., Yokoyama, H. & Naito, M. Homogeneously dispersed polyrotaxane in epoxy adhesive and its improvement in the fracture toughness. *Macromolecules* **52**, 2464–2475 (2019).
183. Wang, P., Gao, Z., Yuan, M., Zhu, J. & Wang, F. Mechanically linked poly[2]rotaxanes constructed from the benzo-21-crown-7/secondary ammonium salt recognition motif. *Polym. Chem.* **7**, 3664–3668 (2016).
184. Zhang, M. et al. Preparation of a daisy chain via threading-followed-by-polymerization. *Macromolecules* **44**, 9629–9634 (2011).
185. Sasabe, H. et al. Synthesis of poly[2]rotaxane by Sonogashira polycondensation. *J. Polym. Sci. A Polym. Chem.* **45**, 4154–4160 (2007).
186. Rotzler, J. & Mayor, M. Molecular daisy chains. *Chem. Soc. Rev.* **42**, 44–62 (2013).
187. Bruns, C. J. & Stoddart, J. F. Rotaxane-based molecular muscles. *Acc. Chem. Res.* **47**, 2186–2199 (2014).
188. Clark, P. G., Day, M. W. & Grubbs, R. H. Switching and extension of a [c2]daisy-chain dimer polymer. *J. Am. Chem. Soc.* **131**, 13631–13633 (2009).
189. Fang, L. et al. Acid-base actuation of [c2]daisy chains. *J. Am. Chem. Soc.* **131**, 7126–7134 (2009).
190. Hmadeh, M. et al. On the thermodynamic and kinetic investigations of a [c2]daisy chain polymer. *J. Mater. Chem.* **20**, 3422–3430 (2010).
191. Guidry, E. N., Li, J., Stoddart, J. F. & Grubbs, R. H. Bifunctional [c2]daisy-chains and their incorporation into mechanically interlocked polymers. *J. Am. Chem. Soc.* **129**, 8944–8945 (2007).
192. Mariani, G. et al. Integration of molecular machines into supramolecular materials: Actuation between equilibrium polymers and crystal-like gels. *Nanoscale* **9**, 18456–18466 (2017).
193. Goujon, A. et al. Controlled sol–gel transitions by actuating molecular machine based supramolecular polymers. *J. Am. Chem. Soc.* **139**, 4923–4928 (2017).
194. Xia, D. & Xue, M. A supramolecular polymer gel with dual-responsiveness constructed by crown ether based molecular recognition. *Polym. Chem.* **5**, 5591–5597 (2014).
195. Bruns, C. J. & Stoddart, J. F. Supramolecular polymers: Molecular machines muscle up. *Nat. Nanotechnol.* **8**, 9–10 (2013).
196. Zhao, Y. L., Zhang, R. Q., Minot, C., Hermann, K. & Van Hove, M. A. Revealing highly unbalanced energy barriers in the extension and contraction of the muscle-like motion of a [c2]daisy chain. *Phys. Chem. Chem. Phys.* **17**, 18318–18326 (2015).
197. Du, G., Moulin, E., Jouault, N., Buhler, E. & Giuseppone, N. Muscle-like supramolecular polymers: Integrated motion from thousands of molecular machines. *Angew. Chem. Int. Ed. Engl.* **51**, 12504–12508 (2012).
198. Goujon, A. et al. Bistable [c2] daisy chain rotaxanes as reversible muscle-like actuators in mechanically active gels. *J. Am. Chem. Soc.* **139**, 14825–14828 (2017).
199. Iwaso, K., Takashima, Y. & Harada, A. Fast response dry-type artificial molecular muscles with [c2]daisy chains. *Nat. Chem.* **8**, 625–632 (2016).
200. Ikejiri, S., Takashima, Y., Osaki, M., Yamaguchi, H. & Harada, A. Solvent-free photoresponsive artificial muscles rapidly driven by molecular machines. *J. Am. Chem. Soc.* **140**, 17308–17315 (2018).
201. Geerts, Y., Muscat, D. & Müllen, K. Synthesis of oligo[2]catenanes. *Macromol. Chem. Phys.* **196**, 3425–3435 (1995).
202. Muscat, D., Witte, A., Köhler, W., Müllen, K. & Geerts, Y. Synthesis of a novel poly[2]-catenane containing rigid catenanes. *Macromol. Rapid Commun.* **18**, 233–241 (1997).
203. Muscat, D. et al. Synthesis and characterization of poly[2]-catenanes containing rigid catenane segments. *Macromolecules* **32**, 1737–1745 (1999).
204. Fustin, C.-A. et al. Mechanically linked polycarbonate. *J. Am. Chem. Soc.* **125**, 2200–2207 (2003).
205. Fustin, C.-A., Bailly, C., Clarkson, G. J., Galow, T. H. & Leigh, D. A. Solution and solid-state properties of mechanically linked polycarbonates. *Macromolecules* **37**, 66–70 (2004).
206. Fustin, C.-A. et al. Mechanically linked poly(ethylene terephthalate). *Macromolecules* **37**, 7884–7892 (2004).
207. Van Quaethem, A., Lussis, P., Leigh, D. A., Duwez, A.-S. & Fustin, C.-A. Probing the mobility of catenane rings in single molecules. *Chem. Sci.* **5**, 1449–1452 (2014).
208. Xing, H., Li, Z., Wu, Z. L. & Huang, F. Catenane crosslinked mechanically adaptive polymer gel. *Macromol. Rapid Commun.* **39**, 1700361 (2018).
209. Ahamed, B. N., Van Velthem, P., Robeyns, K. & Fustin, C.-A. Influence of a single catenane on the solid-state properties of mechanically linked polymers. *ACS Macro Lett.* **6**, 468–472 (2017).
210. Xing, H. et al. Mechanochemistry of an interlocked poly[2]catenane: from single molecule to bulk gel. *CCS Chem.* **1**, 513–523 (2019).
211. Wang, W. & Xing, H. A novel supramolecular polymer network based on a catenane-type crosslinker. *Polym. Chem.* **9**, 2087–2091 (2018).
212. Gan, Y., Dong, D. & Hogen-Esch, T. E. Synthesis and characterization of a catenated polystyrene–poly(2-vinylpyridine) block copolymer. *Macromolecules* **35**, 6799–6803 (2002).
213. Bunha, A. K., Mangadlao, J., Felipe, M. J., Pangilinan, K. & Advincula, R. Catenated PS-PMMA block copolymers via supramolecularly templated ATRP initiator approach. *Macromol. Rapid Commun.* **33**, 1214–1219 (2012).
214. Bunha, A. et al. Polymeric catenanes synthesized via 'click' chemistry and atom transfer radical coupling. *Chem. Commun.* **51**, 7528–7531 (2015).
215. Cao, P.-F., Mangadlao, J. D., de Leon, A., Su, Z. & Advincula, R. C. Catenated poly(ε-caprolactone) and poly(L-lactide) via ring-expansion strategy. *Macromolecules* **48**, 3825–3833 (2015).
216. Ishikawa, K., Yamamoto, T., Asakawa, M. & Tezuka, Y. Effective synthesis of polymer catenanes by cooperative electrostatic/hydrogen-bonding self-assembly and covalent fixation. *Macromolecules* **43**, 168–176 (2010).
217. Ohta, Y., Nakamura, M., Matsushita, Y. & Takano, A. Synthesis, separation and characterization of knotted ring polymers. *Polymer* **53**, 466–470 (2012).
218. Weidmann, J.-L. et al. Poly[2]catenanes and cyclic oligo[2]catenanes containing alternating topological and covalent bonds: synthesis and characterization. *Chem. Eur. J.* **5**, 1841–1851 (2002).
219. Wu, Q. et al. Poly[*n*]catenanes: Synthesis of molecular interlocked chains. *Science* **358**, 1434–1439 (2017).
220. Pakula, T. & Jeszka, K. Simulation of single complex macromolecules. 1. Structure and dynamics of catenanes. *Macromolecules* **32**, 6821–6830 (1999).
221. Rauscher, P. M., Rowan, S. J. & de Pablo, J. J. Topological effects in isolated poly[*n*]catenanes: molecular dynamics simulations and rouse mode analysis. *ACS Macro Lett.* **7**, 938–943 (2018).
222. Amabilino, D. B., Ashton, P. R., Reder, A. S., Spencer, N. & Stoddart, J. F. Olympiadane. *Angew. Chem. Int. Ed. Engl.* **33**, 1286–1290 (1994).
223. Iwamoto, H. et al. Synthesis of linear [5]catenanes via olefin metathesis dimerization of pseudorotaxanes composed of a [2]catenane and a secondary ammonium salt. *Chem. Commun.* **52**, 319–322 (2016).
224. Amabilino, D. B. et al. The five-stage self-assembly of a branched heptacatenane. *Angew. Chem. Int. Ed. Engl.* **36**, 2070–2072 (1997).
225. Watanabe, N., Ikari, Y., Kihara, N. & Takata, T. Bridged polycatenane. *Macromolecules* **37**, 6663–6666 (2004).
226. Brereton, M. G. The statistical mechanics of a concatenated polymer chain. *J. Phys. A Math. Gen.* **34**, 5131 (2001).
227. Ahmadian Dehaghani, Z., Chubak, I., Likos, C. N. & Ejtehadi, M. R. Effects of topological constraints on linked ring polymers in solvents of varying quality. *Soft Matter* **16**, 3029–3038 (2020).
228. Rauscher, P. M., Schweizer, K. S., Rowan, S. J. & de Pablo, J. J. Thermodynamics and structure of poly[*n*]catenane melts. *Macromolecules* **53**, 3390–3408 (2020).
229. Rauscher, P. M., Schweizer, K. S., Rowan, S. J. & de Pablo, J. J. Dynamics of poly[*n*]catenane melts. *J. Chem. Phys.* **152**, 214901 (2020).
230. de Gennes, P.-G. *Scaling Concepts in Polymer Physics* (Cornell Univ. Press, 1979).
231. Raphaël, E., Gay, C. & de Gennes, P.-G. Progressive construction of an "Olympic" gel. *J. Stat. Phys.* **89**, 111–118 (1997).
232. Pickett, G. T. DNA-origami technique for olympic gels. *Europhys. Lett.* **76**, 616–622 (2006).
233. Fischer, J., Lang, M. & Sommer, J.-U. The formation and structure of Olympic gels. *J. Chem. Phys.* **143**, 243114 (2015).
234. Vilgis, T. A. & Otto, M. Elasticity of entangled polymer loops: Olympic gels. *Phys. Rev. E* **56**, R1314–R1317 (1997).
235. Lang, M., Fischer, J., Werner, M. & Sommer, J.-U. Swelling of Olympic gels. *Phys. Rev. Lett.* **112**, 238001 (2014).
236. Lang, M., Fischer, J., Werner, M. & Sommer, J.-U. Olympic gels: concatenation and swelling. *Macromol. Symp.* **358**, 140–147 (2015).
237. Endo, K., Shiroi, T., Murata, N., Kojima, G. & Yamanaka, T. Synthesis and characterization of poly(1,2-dithiane). *Macromolecules* **37**, 3143–3150 (2004).
238. Kim, Y. S. et al. Gelation of the genome by topoisomerase II targeting anticancer agents. *Soft Matter* **9**, 1656–1663 (2013).
239. Arakawa, R., Watanabe, T., Fukuo, T. & Endo, K. Determination of cyclic structure for polydithiane using electrospray ionization mass spectrometry. *J. Polym. Sci. A Polym. Chem.* **38**, 4403–4406 (2000).
240. Endo, K. & Yamanaka, T. Copolymerization of lipoic acid with 1,2-dithiane and characterization of the copolymer as an interlocked cyclic polymer. *Macromolecules* **39**, 4038–4043 (2006).
241. Borst, P. & Hoeijmakers, J. H. J. Kinetoplast DNA. *Plasmid* **2**, 20–40 (1979).
242. Riou, G. & Delain, E. Electron microscopy of the circular kinetoplastic DNA from *Trypanosoma cruzi*: occurrence of catenated forms. *Proc. Natl Acad. Sci. USA* **62**, 210–217 (1969).
243. Cavalcanti, D. P., Gonçalves, D. L., Costa, L. T. & de Souza, W. The structure of the kinetoplast DNA network of *Crithidia fasciculata* revealed by atomic force microscopy. *Micron* **42**, 553–559 (2011).
244. Renger, H. C. & Wolstenholme, D. R. Form and structure of kinetoplast DNA of *Crithidia*. *J. Cell Biol.* **54**, 346–364 (1972).
245. Krasnow, M. & Cozzarelli, N. Catenation of DNA rings by topoisomerases. Mechanism of control by spermidine. *J. Biol. Chem.* **257**, 2687–2693 (1982).
246. Waldeck, W., Theobald, M. & Zentgraf, H. Catenation of DNA by eucaryotic topoisomerase II associated with simian virus 40 minichromosomes. *EMBO J.* **2**, 1255–1261 (1983).
247. Krajina, B. A., Zhu, A., Heilshorn, S. C. & Spakowitz, A. J. Active DNA olympic hydrogels driven by topoisomerase activity. *Phys. Rev. Lett.* **121**, 148001 (2018).
248. Imholt, L. et al. Grafted polyrotaxanes as highly conductive electrolytes for lithium metal batteries. *J. Power Sources* **409**, 148–158 (2019).

Acknowledgements
This work was funded by National Science Foundation (NSF) grant number CHE-1903603. P.M.R. thanks the NSF for the award of a Graduate Research Fellowship, grant number 1746045.

Author contributions
All authors contributed to the writing, reviewing and editing of the manuscript.

Competing interests
The authors declare no competing interests.

Publisher's note
Springer Nature remains neutral with regard to jurisdictional claims in published maps and institutional affiliations.

QUERY FORM

Nature Reviews Materials	
Manuscript ID	**278**
Author	**Laura F. Hart**

AUTHOR:

The following queries have arisen during the editing of your manuscript. Please answer by making the requisite corrections directly in the e.proofing tool rather than marking them up on the PDF. This will ensure that your corrections are incorporated accurately and that your paper is published as quickly as possible.

Query No.	*Nature of Query*
Q1:	Please check your article carefully, coordinate with any co-authors and enter all final edits clearly in the eproof, remembering to save frequently. Once corrections are submitted, we cannot routinely make further changes to the article.
Q2:	Note that the eproof should be amended in only one browser window at any one time; otherwise changes will be overwritten.
Q3:	Author surnames have been highlighted. Please check these carefully and adjust if the first name or surname is marked up incorrectly. Note that changes here will affect indexing of your article in public repositories such as PubMed. Also, carefully check the spelling and numbering of all author names and affiliations, and the corresponding email address(es).
Q4:	In the caption for Fig, 7 panel b, '280 nm' has been changed to '290 nm' on both occurrences, to match the figure image. Please check that this is OK. Also, the occurrence of '280 nm' in the text has been changed to suit as well.